Title

Identifying the Unique Properties of α-Bi2Mo3O12 for the Activation of Propene

Journal

The Journal of Physical Chemistry C, 120(51)

ISSN

1932-7447

Authors

Licht, Rachel B
Getsoian, Andrew Bean
Bell, Alexis T

Publication Date

2016-12-29

DOI

10.1021/acs.jpcc.6b09949

Peer reviewed

Identifying the Unique Properties of α-$Bi_2Mo_3O_{12}$ for the Activation of Propene

Rachel B. Licht, Andrew "Bean" Getsoian, and Alexis T. Bell*

Department of Chemical and Biomolecular Engineering
University of California
Berkeley, CA 94720-1462
and
Chemical Sciences Division
Lawrence Berkeley National Laboratory
Berkeley, CA 94720

Abstract

In order to understand the remarkable activity of α-$Bi_2Mo_3O_{12}$ for selective oxidation and ammoxidation of propene, the propene activation ability of four molybdenum-based mixed metal oxides – $Bi_2Mo_3O_{12}$, $PbMoO_4$, $Bi_2Pb_5Mo_8O_{32}$, and MoO_3 – was investigated using Density Functional Theory. Propene activation is considered to occur via abstraction of a hydrogen atom from the methyl group of physisorbed propene by lattice oxygen. For each material, the apparent activation energy was estimated by summing the heat of adsorption of propene, the C-H bond dissociation energy, and the hydrogen attachment energy (HAE) for hydrogen addition to lattice oxygen; this sum provides a lower bound for the apparent activation energy. It was found that two structural features of oxide surfaces are essential to achieve low activation barriers: under-coordinated surface cation sites enable strong propene adsorption, and suitable 5- or 6-coordinate geometry at molybdenum result in favorable HAEs. The impact of molybdenum coordination on HAE was elucidated by carrying out a molecular orbital analysis using a cluster model of the molybdate unit. This effort revealed that in 5- and 6-coordinate molybdates, oxygen donor atoms *trans* to molybdenyl oxo atoms destabilize the molybdate prior to H addition but stabilize the molybdate after H addition, thereby providing an HAE ~ 15 kcal/mol more favorable than on 4-coordinate molybdate oxo atoms. Bi^{3+} cations in $Bi_2Mo_3O_{12}$ thus promote catalytic activity by providing both strong adsorption sites for propene, and by forcing molybdate into 5-coordinate geometries that lead to particularly favorable values of the HAE.

1. Introduction

Propene oxidation to acrolein and ammoxidation to acrylonitrile are commercially significant processes, each performed on the scale of ~10 billion lbs/year.[1] The catalysts used for these processes are based on bismuth molybdenum oxides, though commercial formulations may include as many as 10 additional elements to improve catalyst activity, selectivity, and lifetime.[2] The best single-phase catalyst for propene oxidation and ammoxidation is considered to be alpha bismuth molybdate, α-$Bi_2Mo_3O_{12}$, though some researchers have suggested that other bismuth molybdate phases, such as β-$Bi_2Mo_2O_9$ and γ-Bi_2MoO_6, exhibit similar activities.[3,4,5] Mechanistic studies of propene oxidation and ammoxidation have therefore focused on the three primary bismuth molybdate phases, with particular emphasis on the α-$Bi_2Mo_3O_{12}$ phase. The activation energy and partial pressure dependencies for both reactions are the same, leading to the conclusion that the rate-limiting step is the same. [6,7,8,9] Both experimental and theoretical studies have identified this step to be the abstraction of a hydrogen atom from the terminal methyl group to produce a physisorbed allyl radical. [10,11,12,13,14] Isotopic labeling studies have shown that the oxygen atoms involved in propene oxidation come from the catalyst surface and not from adsorbed O_2, which only serves to reoxidize the catalyst. [15,16,] The elementary steps by which allyl radicals are converted to acrolein or acrylonitrile have been the subject of a number of studies.[7,17,18,19,20,21]

Considerable effort has been devoted to identifying the characteristics of a mixed metal oxide that make it active for propene oxidation and ammoxidation. While much is known about the structure and electronic properties of bismuth molybdates, the reason why $Bi_2Mo_3O_{12}$ is particularly active remains a subject of discussion.[14,22,23,24,25] The crystal structure of $Bi_2Mo_3O_{12}$ is related to that of the tetragonal mineral scheelite ($CaWO_4$), but with a monoclinic distortion due to the vacancies that result from the replacement of Ca^{2+} with Bi^{3+} ($Bi_{2/3}\varphi_{1/3}MoO_4$ where φ is a

vacancy).[26] The flexibility of the scheelite structure enables the synthesis of many single-phase, solid-solution tri- and tetra-metal oxides, and has therefore formed the basis for much of this work.[27] However, the scheelite structure alone is insufficient for high activity. For example, lead molybdate $PbMoO_4$ crystallizes as a pure scheelite,[28] but is essentially inactive for propene oxidation and ammoxidation.[29] Complete substitution of the Pb^{2+}, e.g. in $Na_{0.5}Bi_{0.5}MoO_4$, produces a similarly inactive material. However, the activity of these materials increases substantially upon addition of a small amount of Bi^{3+}, with the concurrent addition of vacancies, to form $Pb_{1-3x}Bi_{2x}\varphi_xMoO_4$ ($0 < x \leq 0.07$) or $Na_{0.5-3x}Bi_{0.5+x}\varphi_{2x}MoO_4$ ($0 < x \leq 0.17$).[27,30] These findings have led to the conclusion that cation vacancies are required for catalysis and that somehow vacancy sites are responsible for propene activation. It is notable, however, that bismuth addition and vacancy formation occur simultaneously. To decouple the effects of these two parameters, additional experiments have been performed with $Pb_{1-3x}La_{2x}\varphi_xMoO_4$, in which defects are introduced, but not Bi^{3+} cations.[21] The latter system shows no catalytic activity for $0 \leq x \leq 0.04$, suggesting that both Bi^{3+} cations and vacancies together are required for a molybdate catalyst to exhibit high catalytic activity. This hypothesis is further supported by observations that europium molybdate[31] and cerium or lanthanum molybdate,[32] which also crystallize in scheelite-derived structures containing trivalent cations, but with different orderings of cation vacancies, exhibit lower catalytic activities than $Bi_2Mo_3O_{12}$.

Scheelite structures in which molybdenum is partially or completely replaced with another transition metal (i.e., Fe, V, Ga, W) have also been investigated.[33,34] The activation energy of these catalysts for propene oxidation to acrolein correlates very well with the electronic band gap measured by UV-Visible Spectroscopy at reaction temperature or calculated with Density Functional Theory (DFT).[22] This correlation was found to be a consequence of the electronic

structure of the transition state for H abstraction from propene, which was found to involve a singlet-triplet spin crossing where molybdenyl oxo is rehybridized (Mo=O → •Mo–O•) so that it can accept the hydrogen atom removed from the methyl group of propene.[19,38] The band gap is a measure of the singlet-triplet excitation energy, and therefore correlates to the activation energy for a metal oxo to abstract a hydrogen atom from propene. In these catalysts, the chemistry is presumed to occur on oxygen atoms associated with the redox active metal – molybdenum or its replacement transition metal – and not on oxygen atoms associated with the redox inactive bismuth. This hypothesis is supported by both experimental and theoretical investigation, *vide infra.*

Previous work has shown that while both Bi_2O_3 and MoO_3 are essentially inactive for propene oxidation to acrolein or ammoxidation to acrylonitrile, Bi_2O_3 is able to activate propene and produce a small amount of hexadiene,[35] and molybdenum oxide is able to convert allyl radicals generated *in situ* to acrolein.[36] These findings have led to the longstanding hypothesis that oxygen atoms bound to bismuth are responsible for propene activation to generate allyl radical, while oxygen atoms bound to molybdenum, presumably as molybdenyl oxo groups, are responsible for the conversion of allyl radical to acrolein.[37] However, recent XANES studies by our group have shown that this interpretation is not correct. Exposure of $Bi_2Mo_3O_{12}$ to pure propene at 713 K for 24 h results in the reduction of molybdenum from the 6+ to the 4+ oxidation state, but bismuth remains in the 3+ oxidation state.[18] Supporting DFT calculations[19,38] have led us to conclude that oxygen atoms bound to molybdenum atoms perform all of the chemistry in $Bi_2Mo_3O_{12}$. Therefore, the question of why bismuth is necessary for catalysis remains unanswered.

Our recent theoretical work has shown that Bi^{3+} cations electronically perturb the neighboring surface molybdenyl oxo groups and, in doing so, enhance the activity of these sites

for propene activation via abstraction of a hydrogen atom from the methyl group of adsorbed propene.[19] The influence of the Bi^{3+} cations was attributed to electronic repulsion between the bismuth lone pair and an oxygen 2p lone pair, which destabilizes the Mo=O singlet state, and from back donation from the •Mo–O• π^* orbital to the bismuth 6p orbital, which stabilizes the triplet state. The combination of these electronic effects leads to a lower singlet → triplet excitation energy, and thus lowers the transition-state barrier for hydrogen abstraction from propene. However, the magnitude of this effect is estimated to be only ~3 kcal/mol, which is not enough to explain the overall difference in activity between $Bi_2Mo_3O_{12}$ and other molybdenum-oxide-based materials.

The preceding discussion demonstrates that both the composition and structure of mixed metal oxides play an important role in defining the activity of such materials for propene oxidation and ammoxidation. The aim of the present investigation is use DFT calculations to identify the extent to which specific geometric and electronic properties contribute to the activation energy for propene activation. We have focused our investigation on oxides containing molybdenum as the only redox-active metal, thereby allowing us to directly compare the effects of crystal structure, Mo coordination, and the identity of additional elements. The four metal oxides investigated are MoO_3, $Bi_2Mo_3O_{12}$, $PbMoO_4$, and a mixed Pb/Bi molybdate derived from $PbMoO_4$. Together, these different materials represent a range of molybdenum coordination environments (asymmetric 6-, distorted 5-, symmetric 4-, and distorted 4-coordinate), modifying elements (none, Bi, Pb, and both Bi and Pb), and associations between the molybdenum and the modifying element.

2. Methods

2.1 Slab Model Calculations

All calculations were performed using the Vienna *Ab initio* Simulation Package (VASP) version 5.3.5 using the PBE[39] and M06-L[40] functionals. Calculation parameters were based on those detailed in our previous investigation of functionals for modeling properties of reducible transition metal oxides.[38] Plane wave basis sets[41] were used to model valence electrons and projector augmented wave (PAW) functions[42] were used to model the core electrons. The PAW cores were designed for a plane wave cutoff energy of 400 eV and this cutoff was used for all calculations. Energies were converged with a Gaussian energy smearing of 0.05 eV. In all cases, a converged PBE wave function was used as the initial guess for the final M06-L calculation, since the M06-L functional performs poorly with the default random number initial guess of the wave function.

The atomic positions for bulk $Bi_8Mo_{12}O_{48}$, $Pb_4Mo_4O_{16}$ and Mo_4O_{12} were taken from literature.[26,28,43] The total energy for each literature crystal structure with respect to the gamma k-point mesh was converged to within 0.5 meV/atom. Bulk $Bi_8Mo_{12}O_{48}$ required 3x2x2 k-points, bulk $Pb_4Mo_4O_{16}$ 4x4x2 k-points, and bulk Mo_4O_{12} 6x2x6 k-points. Using these k-point grids, the atomic positions of each structure were then allowed to relax at a series of fixed volumes. The Burch-Murnaghan Equation of State[44] was used to fit the data of energy versus volume and calculate the cell volume with the minimum energy. The atoms were then allowed to relax at this fixed minimum energy volume until the total energy converged to within 0.1 meV. The optimized cell volume was found to be 2.3% larger than the experimental value $Bi_8Mo_{12}O_{48}$, 1.6% smaller for $Pb_4Mo_4O_{16}$, , and 4.8% smaller for Mo_4O_{12}.

Both alpha bismuth molybdate and molybdenum trioxide have one crystallographic axis along which there are four layers, with each pair of layers strongly bound together and weaker bonds between the paired layers, and only strong bonds between atoms in the other two

crystallographic directions. Cleaving the crystal between the weakly bonded layer pairs is, therefore, the most obvious way to produce a surface with the lowest energy. The resulting surface is the (010) surface for both alpha bismuth molybdate and molybdenum trioxide. Lead molybdate also has four layers in the direction perpendicular to the (001) plane, which, because of crystallographic naming conventions, is the pure scheelite plane that is equivalent to the (010) plane in the distorted scheelite alpha bismuth molybdate. Therefore, for consistency in comparison with alpha bismuth molybdate, we used the (001) surface of lead molybdate, which is also the principal plane observed experimentally after cooling a $PbMoO_4$ melt.[45] The optimized bulk structures were cleaved to create the relevant surface plane terminated with a full complement of oxygen atoms. 14 Å of vacuum space was added above the atoms to create a surface, and, in all cases, only 1 k-point was used in the direction perpendicular to the surface. The top two layers were allowed to relax to a convergence of 0.5 meV total energy, while the bottom two layers were fixed in their bulk positions to simulate the bulk oxide below the surface.

The crystallographic unit cells of both lead molybdate and molybdenum oxide only contain one molybdenum atom in each layer, which, because of the periodic boundary conditions, results in the effective reduction of every surface molybdenum atom upon attachment of only one hydrogen atom. To avoid this, for both materials, multiple unit cells were combined to make a supercell that was used to model the oxide surface. Two unit cells were combined to represent $Pb_8Mo_8O_{32}$, which has two surface Mo atoms and two surface Pb atoms. The resulting (001) surface plane is a 59.4 $Å^2$ square that needed 3x3x1 k-points to yield converged energies. Four unit cells were combined to create $Mo_{16}O_{48}$, which has four Mo atoms on the (010) surface forming an almost square surface also with area 59.4 $Å^2$. Calculations on this slab were performed at 3x1x3 k-points. For comparison, $Bi_8Mo_{12}O_{48}$ has three surface Mo atoms, two surface Bi atoms, and has

a rhombohedral surface with an area of 83.9 $Å^2$. Slab calculations on this (010) surface employed 3x1x2 k-points. The Minnesota family of functionals requires a fine integration grid to provide accurate energies, [46] therefore an integration grid of 1 point per each ~0.085Å in each crystallographic direction was used (90x288x144 for $Bi_8Mo_{12}O_{48}$, 90x90x300 for $Pb_8Mo_8O_{32}$, and 90x324x90 for $Mo_{16}O_{48}$). We defined the number of bands explicitly to account for all of the electron pairs in each bulk surface plus an additional ~20% of empty valence bands (240 bands for $Bi_8Mo_{12}O_{48}$, 168 for $Pb_8Mo_8O_{32}$ and 240 for $Mo_{16}O_{48}$). The added bands are essential in order to include all of the unoccupied d orbital states on each Mo in the calculation, so that the band gap and conduction band states (including the LUMO) are properly described.

We also generated a mixed bismuth/lead material with the unit cell $Pb_5Bi_2Mo_8O_{32}$. According to the phase diagram for $Pb_{1-3x}Bi_{2x}\varphi_xMoO_4$, a single phase scheelite material can exist up to $x \approx 0.15$, though only at specific temperatures (i.e. only ~970 K for $x \approx 0.15$).[47] Above $x \approx 0.15$ or at other temperatures, this material will separate into a mixed scheelite and $Bi_2Mo_3O_{12}$. Our model compound $Pb_5Bi_2Mo_8O_{32}$ ($x = 0.125$), would be difficult to maintain in a single-phase solid solution; however, it is known to exist[47] and it is the only mixed Pb/Bi molybdate that can be easily generated from the pure scheelite lead molybdate without requiring a computationally infeasible number of atoms in the unit cell. $Pb_5Bi_2Mo_8O_{32}$ was made by replacing three lead atoms in the bulk $Pb_8Mo_8O_{32}$ with two bismuth atoms and one vacancy. One bismuth atom and one lead atom were placed at what would become the surface, one lead and the vacancy were placed in the layer below, and finally one lead atom and the last bismuth atom were placed in the layer below the vacancy. Bulk $Pb_5Bi_2Mo_8O_{32}$ required 3x3x2 k-points (crystallographic axes the same as lead molybdate). The optimal cell volume was found by allowing the atoms to relax with a series of fixed tetragonal cell volumes and fitting the volume versus energy with the Burch-Murnaghan

Equation of State to find the optimal cell volume. The experimentally-measured cell volume of $Pb_{0.64}Bi_{0.24}MoO_4$, which is very similar to our model compound ($Pb_{0.625}Bi_{0.25}MoO_4$), is 2.5% smaller than that of $PbMoO_4$,[47] since bismuth cations have a smaller radius than lead cations. In excellent agreement with these experimental results, we calculated the DFT optimized cell volume of $Pb_5Bi_2Mo_8O_{32}$ to be 2.5% smaller than the DFT optimized cell volume of $PbMoO_4$. It should be noted that no monoclinic distortion has been observed experimentally for any single-phase mixed Pb/Bi material,[47] so we fixed our model compound $Pb_5Bi_2Mo_8O_{32}$ to have tetragonal symmetry while changing the volume and optimizing the atom positions. Once the bulk $Pb_5Bi_2Mo_8O_{32}$ was optimized, the (001) surface was generated and optimized in the same way as $Pb_8Mo_8O_{32}$ (see above).

Finally, we tested substituted bismuth molybdate structures where one bismuth atom was replaced by one atom of a different element in order to determine the effect of that atom. For these structures, the optimized surface of $Bi_8Mo_{12}O_{48}$ was used as the starting structure, and then the entire surface was allowed to relax to within 0.5 meV with the relevant surface bismuth atom replaced by another element. Since lead has a different oxidation state than bismuth (2+ versus 3+), a hydrogen atom was also included in the former case in order to balance the charge (i.e., $PbHBi_7Mo_{12}O_{48}$). The other elements tested were all in the 3+ oxidation state (Sb, B, La).

2.2 Cluster model calculations

In order to examine the molecular orbitals around molybdenum for different bonding configurations, we carried out model cluster calculations using quantum chemical methods contained in the Q-Chem software package, version 4.2.3.[48] The Def2-TZVPD effective core potential and valence basis set,[49] obtained from the EMSL basis set exchange,[50] was used for molybdenum and the 6-311++G(3df,3pd) basis set was used for oxygen, hydrogen and carbon.

The M06-L exchange-correlation functional[40] was employed to obtain the final cluster and orbital energies presented here. The results were also compared to calculations with the PBE functional[39] and with the ωB97X functional, both with and without dispersion (ωB97X-D),[51] and verified to show the same trends. Molecular orbitals were extracted using MolDen,[52] and electron density plots prepared with Vesta.[53]

A 4-coordinate $MoO_2(OH)_2$ cluster and a 5-coordinate $MoO_2(OH)_2$-$O(CH_3)_2$ cluster, where in the later case the dimethyl ether (DME) is orientated such that the oxygen is pointing towards the molybdenum to mimic a fifth coordination site, were individually optimized both with and without an added hydrogen. For both clusters, the same torsional angle constraint on both side hydroxyl groups (116.4° for O_{Cis}-Mo-O-H) was used to prevent the hydrogen atoms from engaging in spurious hydrogen bonding with the oxo groups, since those hydrogen atoms are merely there to terminate the cluster. In order to extract the molecular orbital energies for the optimized clusters after hydrogen addition, the geometry was frozen, the hydrogen removed, and the orbitals calculated in the spin singlet state. For the plots of energy versus Mo-O_δ distance, the cluster was allowed optimize with the constraint that the Mo-O_δ distance remained fixed.

DME was chosen to mimic the fifth coordination site because it provides a 2-coordinate oxygen moiety that is small and does not add obfuscating hydrogen bonding effects. DME is admittedly not a perfect model of the Bi–O–Mo arrangement that is the fifth coordination site in $Bi_2Mo_3O_{12}$, but, by using DME, we are able to isolate the effect of bringing an additional oxygen coordination close to the molybdenum without significantly perturbing the rest of the molybdate cluster in any way. For this reason, we do not attempt to directly compare the results of the cluster calculations and the slab calculations, but merely extend the findings from the cluster calculations to explain what we observe in the slab calculations.

3. Results and Discussion

3.1 Key Energy Parameters

We propose that an active catalyst for propene oxidation and ammoxidation must have (1) an active oxygen atom for hydrogen abstraction and (2) a favorable propene adsorption site near the active oxygen atom. In order to probe these features for $Bi_2Mo_3O_{12}$, $PbMoO_4$, $Bi_2Pb_5Mo_8O_{32}$ and MoO_3, we will reference the energies shown in Fig. 1, so that for each material, zero relative energy is the bare oxidized surface plus propene in the gas phase. $\Delta E_{ads,C3H6}$ is the energy change upon propene adsorption on the oxidized surface and will always be a negative number. ΔE_{rxn} is the overall energy of reaction to go from adsorbed propene to adsorbed allyl radical and a hydrogen atom added to a Mo=O group. This hydrogen abstraction process has an activation barrier, shown in grey in Fig. 1. The transition-state energy is designated as ΔE_{TS}. At the high temperature required for propene oxidation and ammoxidation (~ 600-700 K), entropy dominates adsorption, and the catalyst resting state is the bare oxidized surface plus gas-phase propene. Therefore, as indicated by $E_{a,app}$ in Fig. 1, the apparent activation energy for hydrogen abstraction from propene will be the energy difference between the transition state and the bare oxidized surface with propene in the gas phase.

We have previously calculated the activation barrier for hydrogen abstraction from propene adsorbed on $Bi_2Mo_3O_{12}$ to be ΔE_{TS} = 38.8 kcal/mol.[17] This reaction occurs via a singlet-triplet spin-crossing transition state that is only 7.6 kcal/mol above the final state. In the final state, the allyl radical is weakly adsorbed on the oxide surface and has a geometry and energy that are quite similar to those of the transition state. Since determination of the transition state is computationally very intensive, in part due to the slow convergence characteristics of calculations done using the

M06-L functional, we chose to compare the properties of different oxides on the basis of the structure and energy of the final state attained after hydrogen abstraction from propene and to use this energy as a measure of the relative apparent activation energies for hydrogen abstraction from propene on different oxides. We note that the energy of the final state is clearly a lower bound on the apparent activation energy, since the transition state must be higher in energy than the energy of the final state. As will be shown below, calculation of this lower bound is sufficient for comparing the catalytic activity of different molybdate phases.

Another metric we will use is the Hydrogen Attachment Energy (HAE), which is a measure of the hydrogen abstraction ability of various surface oxygen atoms. The HAE is defined as the energy difference between an all-electron-paired bare catalyst surface plus a gas phase hydrogen atom (with a single electron) and the catalyst surface with the hydrogen atom attached to a surface oxygen and thus one unpaired electron, as in Eqn (1).

$$HAE = E_{H\text{-}surf} - (E_{surf} + E_H) \quad (1)$$

Fig. 1 demonstrates that the energy of the final state is the sum of HAE, the bond dissociation energy of a hydrogen on the methyl group of propene $E_{C\text{-}H}$, and the adsorption energy for the allyl radical $\Delta E_{ads,C3H5}$. Since $E_{C\text{-}H}$ it is independent of the catalyst and $\Delta E_{ads,C3H5}$ is expected to be similar in magnitude to the propene adsorption energy $\Delta E_{ads,C3H6}$, we will use the HAE to determine the most active surface oxygen atom on each material.

There is precedent in the literature for using hydrogen attachment energy as an approximation for C-H bond activation activity, specifically in the area of methane activation. For example, high-level theory calculations reported by Sauer *et al.* demonstrate a good correlation between the hydrogen attachment energy and apparent activation barrier for hydrogen abstraction from both H_2 and CH_4 by metal oxide clusters containing 2-7 metal atoms,[54] as do additional gas

phase methane activation calculations by other researchers.[55] In the field of propane ammoxidation, a strong correlation was observed between the sum of C-H BDE and ΔE of H addition for DFT calculations involving the Mo-V-Te-Nb-O M1 phase.[56] Additionally, previous work in our own group modeling $Bi_2Mo_3O_{12}$ with a less accurate density functional showed that the surface oxygen atom with the lowest HAE had the lowest reaction barrier for hydrogen abstraction from propene, though the reaction barriers for the less active surface oxygen atoms did not track with the HAE.[19] Therefore, though the HAE is not a perfect representation, because of its significantly lower computational requirements, calculations of the HAE provide a reasonable starting point for investigating the activity of a material for C-H bond activation.

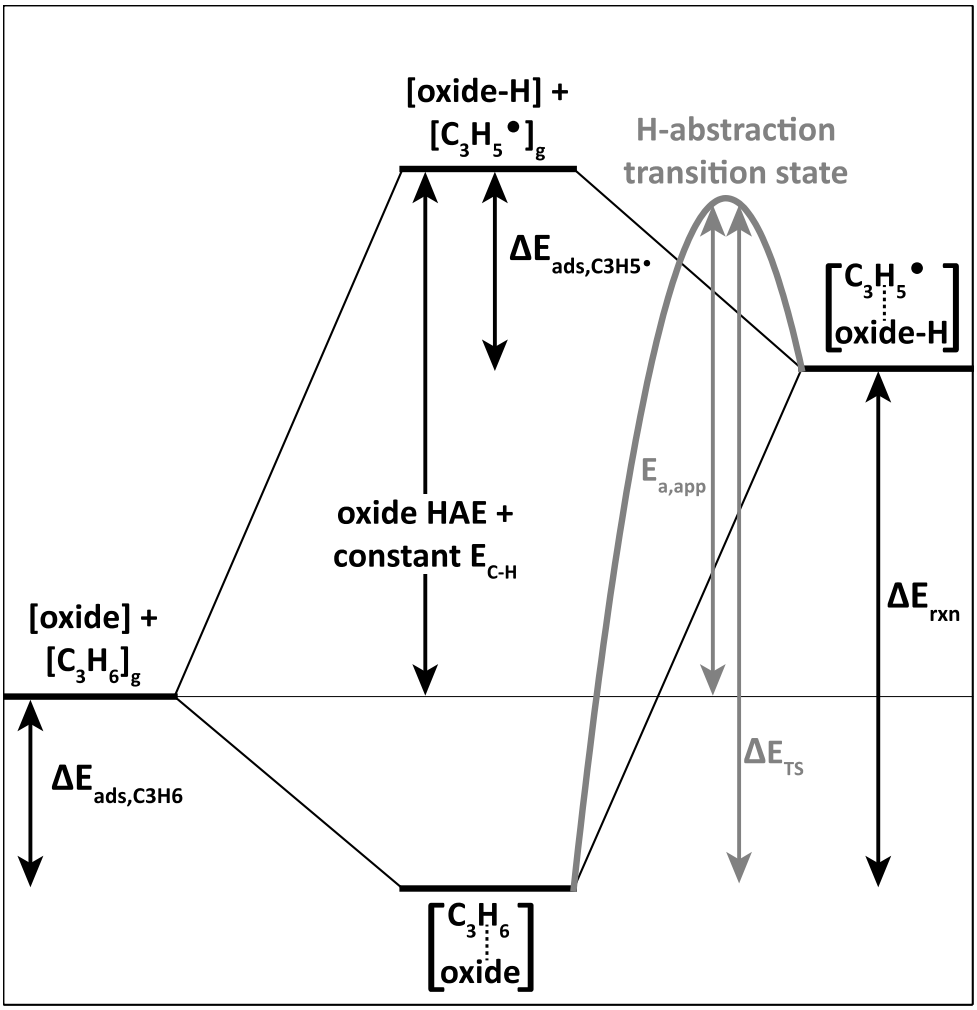

Fig. 1 Diagram depicting the various calculated energy values used throughout this paper.

3.2 Types of Surface Oxygen Atoms

As noted in Table 1, there are different types of oxygen atoms on the surface of the oxides studied, which can be grouped into four general categories. The first type, O_α, is a pure molybdenum-oxygen double bond with a bond length less than or equal to 1.70 Å. The second type, O_β, is an oxygen atom doubly bonded to Mo that is electronically perturbed by a neighboring atom (X), resulting in a slightly longer Mo-O distance, between 1.70 and 1.76 Å. The third type, O_γ, has two single bonds to two different atoms (Mo and X), resulting in a molybdenum-oxygen distance of 1.76-2.00 Å. Finally, the fourth type, O_δ, has two single bonds to two atoms and is also loosely coordinated to a nearby molybdenum atom at a distance of 2.00-2.40 Å. Beyond a Mo-O distance of 2.40 Å, there is no specific interaction between the two atoms.

Oxygen Name	Mo–O distance (d) range [Å]	Depiction	Description
O_α	≤ 1.70	Mo═O	Pure double bond
O_β	$1.70 < d < 1.76$	Mo═O----X	Electronic perturbation by X
O_γ	$1.76 \leq d < 2.00$	Mo—O—X	Two single bonds
O_δ	$2.00 \leq d < 2.40$	Mo----O⟍⟋	Loose coordination

Table 1. Types of surface oxygen atoms, where X can be either Mo or another atom.

3.3 Hydrogen Addition to Oxide Surfaces

In the following subsections, we present the HAE (Table 2) and the surface geometry before and after hydrogen addition for each of the four metal oxide materials (Figs. 2-7). These data can be used to identify what geometries lead to a low HAE. As will be shown, increased coordination of molybdenum 6+ cations by oxygen anions significantly lowers the value of the

HAE. We also find that the ability of the surface to distort upon hydrogen addition and therefore coordinate molybdenum with an additional bulk oxygen atom positioned *trans* to the oxygen atom to which the hydrogen was added is crucial for achieving a favorable HAE.

Material	**Type of Surface Oxygen**	**HAE (kcal/mol)** Full surface relaxation *[hydroxyl relaxation only]*
$Bi_2Mo_3O_{12}$	O_α **O_β** O_γ	-52.9 *[-45.8]* **-58.3** ***[-47.2]*** -45.5
$PbMoO_4$	O_β	-44.0
$Bi_2Pb_5Mo_8O_{32}$	O_β **O_β'** O_β" O_γ	-44.7 **-47.6** ***[-40.3]*** -43.4 -43.9
MoO_3	**O_α** O_β	**-58.2** ***[-54.8]*** -63.2 *[-36.1]*

Table 2. Hydrogen addition energy (HAE) to every type of surface oxygen for the 4 tested mixed metal oxide slab materials (Bolded lines are for the O atom used in Fig. 12).

3.3.1 Alpha Bismuth Molybdate

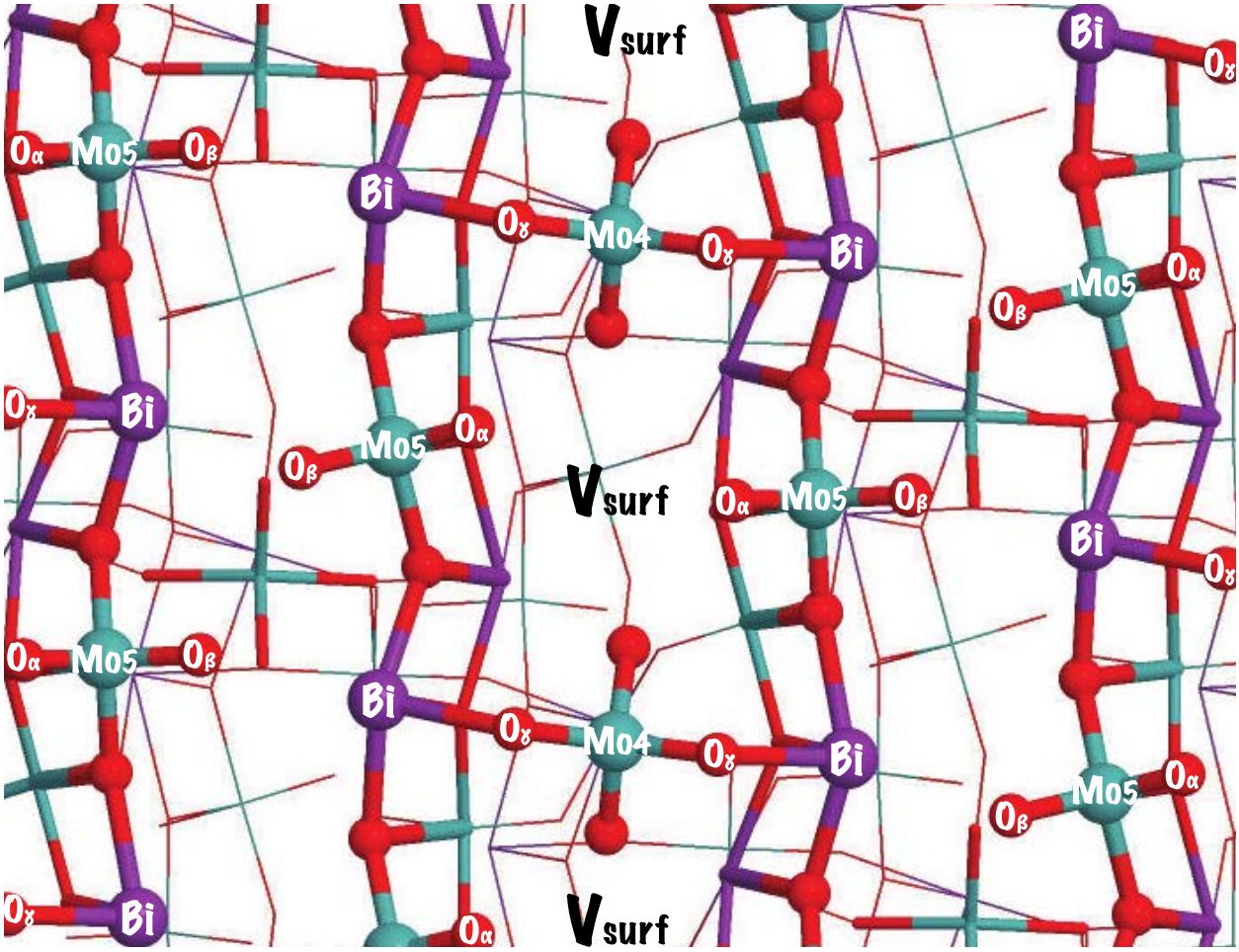

Fig. 2 Top down view of $Bi_2Mo_3O_{12}$, where Mo atoms are turquoise, Bi are purple, and O are red, and the location of surface cation vacancies are indicated by V_{surf}. Surface atoms are identified in white (see Table 1 for explanation of oxygen types).

A top-down view of the lowest energy (010) surface of $Bi_2Mo_3O_{12}$ is shown in Fig. 2 with the ordered cation vacancies indicated with "V_{surf}" and a side view is shown in Fig. 3a. The pseudo-5-coordination of molybdenum and asymmetrical 8-coordination of bismuth in bulk $Bi_2Mo_3O_{12}$ result in two general types of surface molybdenum atoms and three types of surface oxygen atoms. Two thirds of the surface molybdenum atoms are 5-coordinate (Mo_5), formally doubly bonded to two oxygen atoms at the surface (1 O_α and 1 O_β), singly bonded to two oxygen atoms within the surface that connect to neighboring metal atoms, and loosely coordinated to a fifth oxygen atom located beneath the molybdenum (O_δ) that is singly bound to two subsurface metal atoms. The O_α is a pure molybdenyl oxo on the cation vacancy side, while the O_β is electronically perturbed by the neighboring Bi^{3+} cation. As shown in Fig. 3a, surface Bi^{3+} cations are bonded (Bi-O distance 2.1-2.4Å) to four oxygen atoms on one side of itself and coordinated (Bi-O distance 2.5-3.0Å) to two oxygen atoms on its other side, one of which is the surface O_β, but are missing two additional coordinated oxygen atoms they would have in the bulk. The remaining one third of the molybdenum atoms are 4-coordinate (Mo_4), with two singly bonded surface oxygen atoms connected to neighboring metal atoms (O_γ) and two doubly bonded oxygen atoms located below the surface. In the bulk, these Mo_4 atoms would have a fifth loosely coordinated oxygen atom, which is absent at the surface.

Fig. 3b illustrates the geometry at Mo_5 after addition of a hydrogen atom to O_β, Fig. 3c the geometry after addition of a hydrogen atom to O_α, and Fig. 3d the geometry at Mo_4 after addition to O_γ. We observe that the addition of hydrogen atom to the bismuth perturbed molybdenyl oxo O_β, causes the molybdenum atom to sink into the catalyst (Fig. 3b). This movement results in the

formation of a full single bond between the molybdenum and the oxygen (O_δ) *trans* to the position where the hydrogen atom is added, which was previously only loosely coordinated to molybdenum. Similar movement is observed after hydrogen atom addition to the pure molybdenyl oxo, O_α. Again, the molybdenum atom attempts to coordinate with a bulk oxygen atom *trans* to where hydrogen is added; however, that oxygen starts 2.91 Å away from the molybdenum and is therefore only able to achieve a final distance of 2.39 Å after significant surface deformation. Table 2 shows that hydrogen addition to O_β is favored by 5.4 kcal/mol over O_α. By adding a hydrogen atom to either O_α and O_β and only allowing the hydroxyl group to relax while forcing the rest of the atoms to remain in their optimized oxidized surface positions (see bracketed numbers in Table 2), we determined that the more favorable value of HAE for hydrogen addition to O_β is mostly due to the ability of the surface to relax to a final geometry with lower energy.

Hydrogen addition to O_γ is significantly less favorable than addition to either O_α or O_β, as can be seen from Table 2. In contrast to H addition at O_α or O_β, which results in replacement of a Mo=O π bond by an O-H σ bond, H addition at O_γ involves replacement of a Bi-O σ bond by an O-H σ bond, which is less exothermic. After addition to O_γ, the molybdenum it is bound to barely moves and remains purely 4-coordinate, while the bismuth that O_γ is also bound to moves significantly to break the Bi-O_γ bond. In moving away from O_γ, the already under-coordinated bismuth becomes even more under-coordinated, which is also energetically unfavorable.

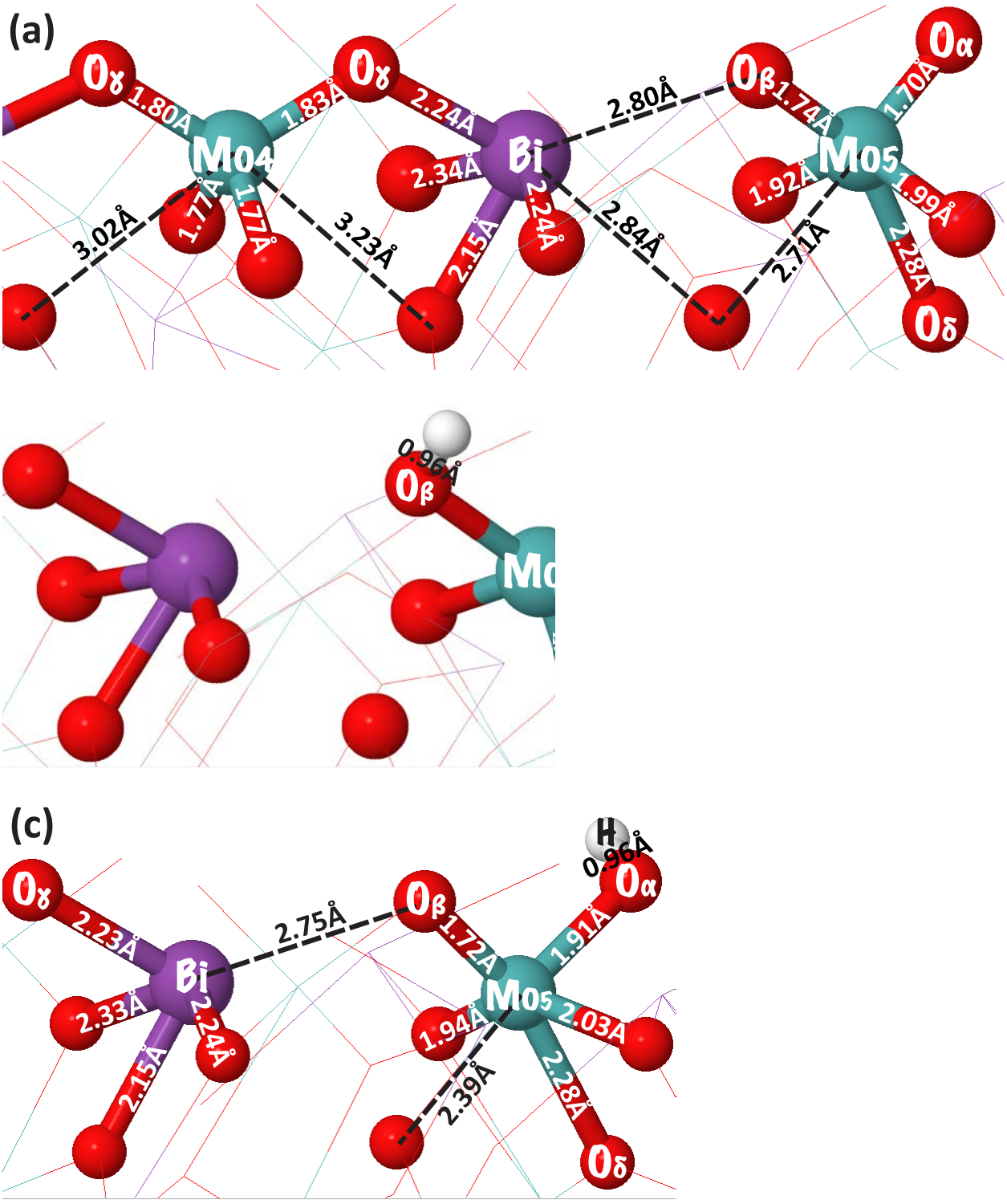
(a)
Oγ
1.80Å
Mo4
1.83Å
Oδ
2.24Å
Bi
2.80Å
Oβ
1.74Å
Mo5
1.70Å
Oα
2.34Å
1.77Å
1.77Å
3.02Å
3.23Å
2.15Å
2.24Å
2.84Å
1.92Å
1.99Å
2.71Å
2.28Å
Oδ
0.96Å
Oβ
Mo
(c)
Oγ
2.23Å
Bi
2.75Å
Oβ
1.72Å
H
0.96Å
Oα
1.91Å
Mo5
2.03Å
2.33Å
2.24Å
2.15Å
1.94Å
2.39Å
2.28Å
Oδ

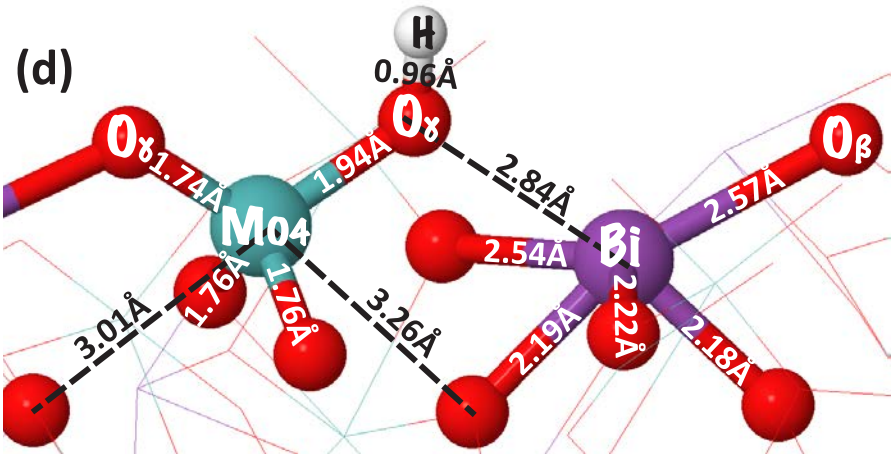

Fig. 3 (a) Side view of optimized (010) surface of $Bi_2Mo_3O_{12}$ showing the three distinct types of surface oxygen atoms and the two distinct types of surface molybdenum atoms. (b) After addition of a hydrogen atom to O_β. (c) After addition of a hydrogen atom to O_α. (d) After addition of a hydrogen atom to O_γ. Relevant distances in Å are indicated on the bond or with a dashed line between atoms.

The calculation of a lower barrier for propene activation at O_β vs O_α has been attributed previously to the influence of a neighboring Bi^{3+} cation on the O_β site.[19] The importance of this effect was investigated in greater detail in the present study. Structures were generated in which one surface Bi^{3+} cation in $Bi_2Mo_3O_{12}$ was replaced by another metal cation X, and the surface was allowed to relax. The rest of the $Bi_2Mo_3O_{12}$ structure was fixed in order to isolate the effect of the perturbing element on hydrogen addition to O_β. In addition to Bi^{3+}, which is known to form a stereochemically active lone pair,[57,58] we also investigated the effects of B^{3+}, La^{3+}, Pb^{2+} plus H^+, and Sb^{3+}. The HAE values and X-O_β distances are given in Table 3, and structural diagrams are given in the Supporting Information. The values of the HAE are found to vary only slightly, despite significant differences in the X-O_β distance, the size of the X cation, the coordination geometry of X, the existence of a stereochemically active lone pair on X, and the oxidation state of X. Substitution of B^{3+} is especially telling, as this cation is too small and too far away to have any interaction with O_β, yet the HAE is only 3 kcal/mol higher in energy than that for the native $Bi_2Mo_3O_{12}$. Therefore, it appears that the favorable molybdenum coordination is the principal

cause for the low HAE of O_β in $Bi_2Mo_3O_{12}$, and the electronic perturbation by a nearby asymmetrically coordinated cation is only a secondary effect.

Perturbing Element (X)	HAE to O_β [kcal/mol]	X-O_β on oxidized surface [Å]
Bi^{3+}	-58.3	2.80
B^{3+}	-55.5	3.95
La^{3+}	-59.9	2.50
$Pb^{2+} + H^{+}$	-59.4	2.79
Sb^{3+}	-56.7	3.01

Table 3. Hydrogen Attachment Energy (HAE) and X-O_β distance on the oxidized surface for different perturbing elements (X) replacing one surface Bi^{3+} in the (010) surface of $Bi_2Mo_3O_{12}$.

3.3.2 Lead Molybdate

Molybdenum atoms in bulk $PbMoO_4$ are tetrahedrally coordinated to four oxygen atoms located at 1.77 Å, and the lead atoms fill the voids between eight tetrahedral units. On the optimized surface, the molybdenum atoms remain symmetric, but move slightly closer to the surface. Per molybdenum, this results in two singly bonded oxygen atoms below the surface and two equivalent doubly bonded oxygen atoms at the surface (O_β) that are electronically perturbed by nearby surface lead atoms, each of which is bound to four subsurface oxygen atoms.

Addition of a hydrogen atom to any of the equivalent surface O_β oxygen atoms distorts the oxygen out of the surface and away from the neighboring lead atom (see Fig. 4b). Similarly to what was observed in $Bi_2Mo_3O_{12}$ after hydrogen addition, the molybdenum atom relaxes back towards the next nearest oxygen atom that is *trans* to the oxygen atom where the hydrogen was added. However, since the molybdenum was not initially close to this atom, after surface optimization it is still 2.67 Å away. As seen in Table 2, addition of a hydrogen atom to O_β of $PbMoO_4$ is much less favorable than addition to either O_α or O_β of $Bi_2Mo_3O_{12}$. We attribute this to

the inability of the 4-coordinate Mo in $PbMoO_4$ to form a strong association with another oxygen atom upon addition of the hydrogen atom, as explored further below.

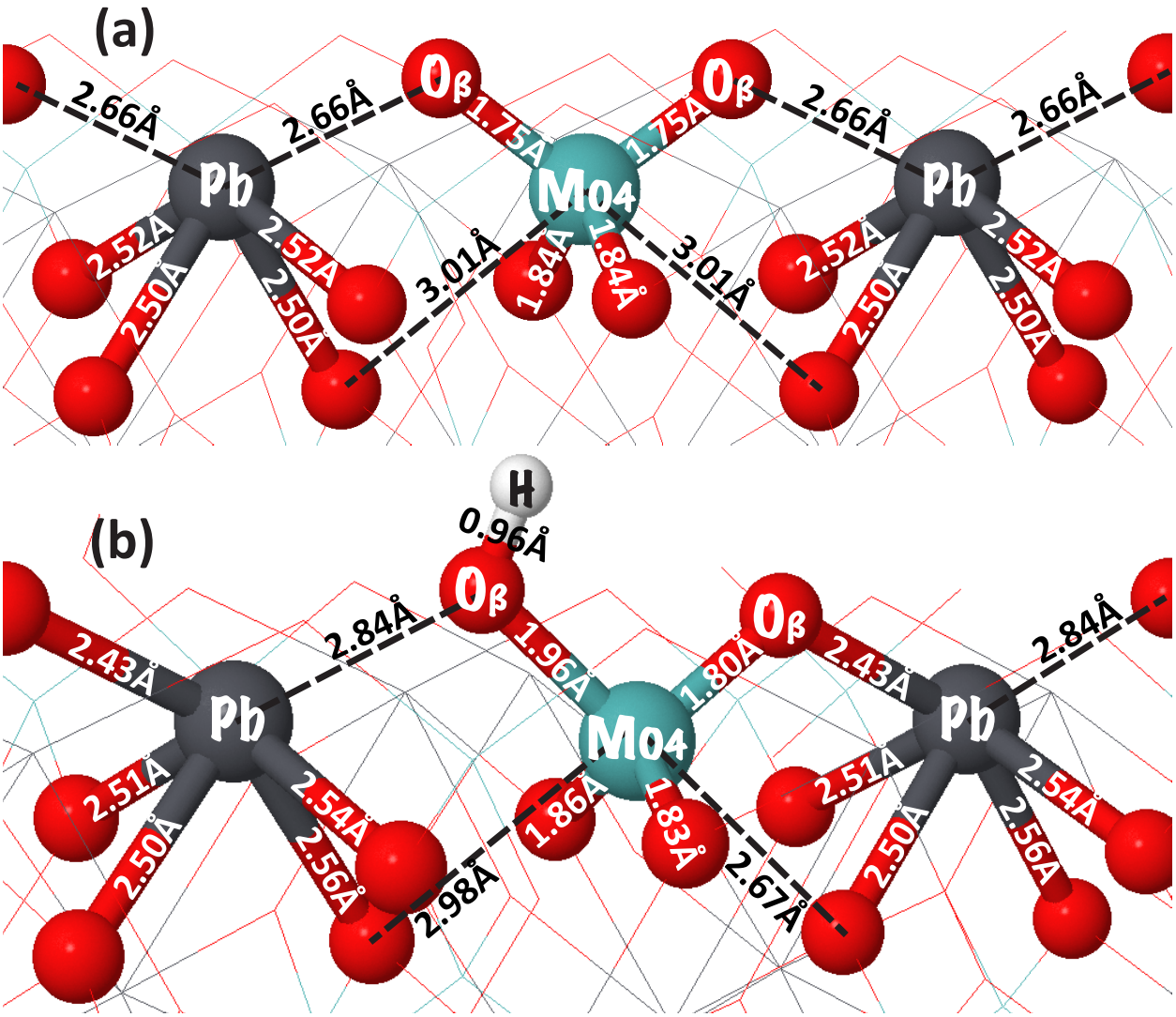

Fig. 4 (a) Side view of the fully oxidized surface of $PbMoO_4$. (b) The same view after hydrogen addition to one of the equivalent O_β atoms. Relevant distances in Å are indicated on the bond or with a dashed line between atoms.

3.3.3 Bismuth/Lead Mixed Molybdate

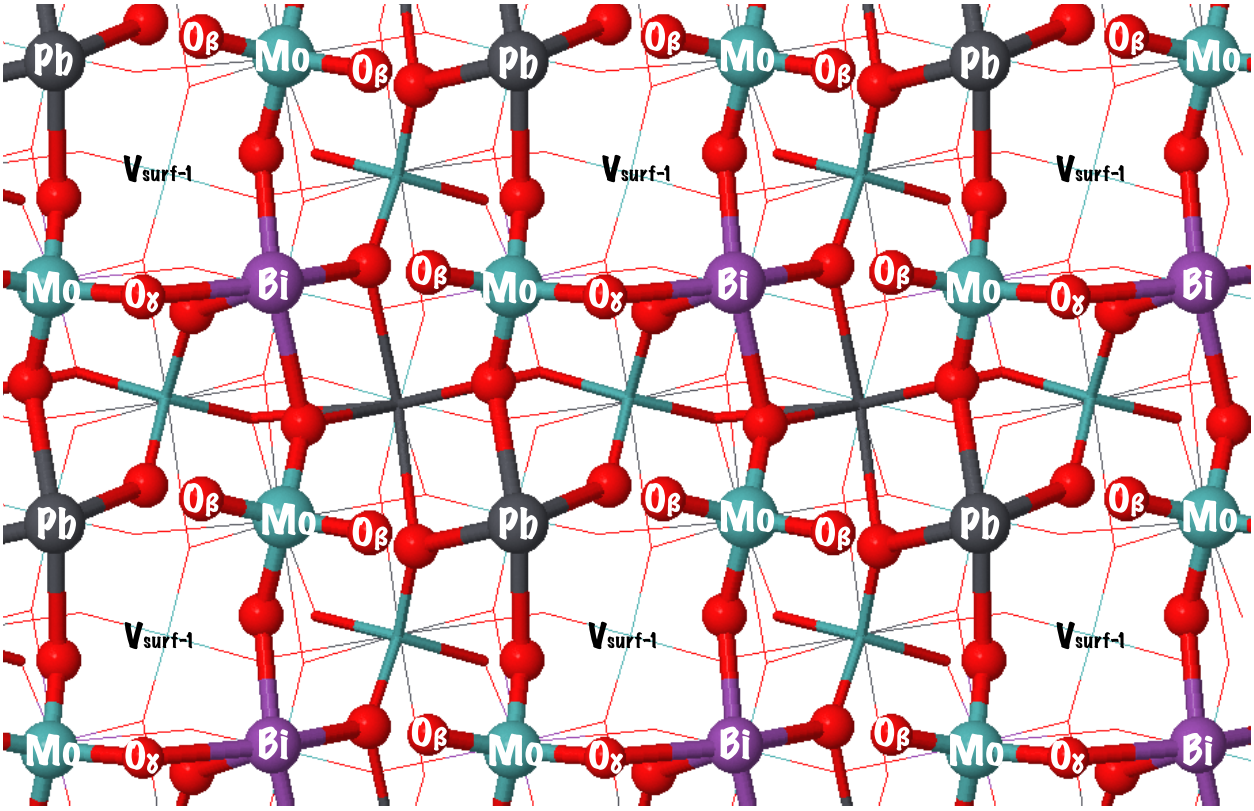

Fig. 5 Top down view of $Bi_2Pb_5Mo_8O_{32}$, where the location of cation vacancies one layer below the surface are indicated by $V_{surf\text{-}1}$. Surface atoms are identified in white (see Table 1 for explanation of oxygen types).

We built a mixed bismuth lead molybdate with the formula $Bi_2Pb_5\varphi_1Mo_8O_{12}$ (φ = cation vacancy) to explore the effect of distorting the pure scheelite $PbMoO_4$. As shown in Fig. 5, this material contains 1:1 ratio of bismuth to lead at the surface, with alternating rows of molybdenum/lead and molybdenum/bismuth. The lattice contains 50% cation vacancies in the layer below the surface (indicated in Fig. 5 by $V_{surf\text{-}1}$), a 1:1 ratio of bismuth to lead in the layer below that, and a full complement of lead cations in the bottom most layer. Note that, since no monoclinic distortion was observed spectroscopically in mixed bismuth lead molybdates with similar concentrations,[47] we constrained the $Bi_2Pb_5\varphi_1Mo_8O_{12}$ to remain in a tetragonal unit cell similar to that of the parent $PbMoO_4$.

Fig. 6a shows a side view of both a lead-molybdenum row and a bismuth-molybdenum row at the surface of $Bi_2Pb_5Mo_8O_{12}$. The surface molybdenum atoms are 4-coordinate, though somewhat distorted from the symmetric tetrahedra observed in the parent $PbMoO_4$. Both bismuth and lead are observed to have an asymmetrical coordination at the surface, with bismuth bonded to five oxygen atoms and lead to four. However, since lead is a larger cation than bismuth, it has significantly longer bonds to its neighboring oxygen atoms and thus ends up modifying the neighboring molybdate unit differently than does bismuth. Molybdenum atoms in the lead row have two doubly bonded surface oxygen atoms that are both electronically perturbed by neighboring lead atoms, but are not equivalent and are therefore designated O_β' and O_β". Molybdenum atoms in the bismuth row have a single bond to a surface bridging oxygen atom also bound to bismuth (O_γ) and one doubly bonded oxygen atom electronically perturbed by a neighboring bismuth atom (O_β).

The HAE values for all four types of surface oxygen atoms are given in Table 2 and the geometry for the lowest energy O_β' in Fig. 6b (geometries for the remaining structures are in the

Supporting Information Fig. S1). Upon hydrogen addition to O_β', the surface undergoes significant geometric distortion such that the molybdenum draws 0.6 Å nearer to an oxygen atom *trans* to O_β' and thus is able to loosely coordinate with it. Even though the molybdenum environment in the lead row of $Bi_2Pb_5Mo_8O_{12}$ starts very similar to the molybdenum environment in $PbMoO_4$, the additional flexibility in the former crystal, due to the introduction of vacancies and the different ionic radii of Bi^{3+} and Pb^{2+}, allows the molybdenum to move and therefore adopt a more favorable conformation upon hydrogen addition. The importance of the geometric distortion with hydrogen addition is obvious from the 7 kcal/mol difference in HAE between hydroxyl relaxation only and full surface relaxation. The HAE value for addition to O_β' is similar to the hydroxyl-relaxation-only HAE for addition to O_β of $Bi_2Mo_3O_{12}$, which without surface relaxation has a similar geometry to the geometry attained after full surface relaxation of hydrogen addition to O_β'.

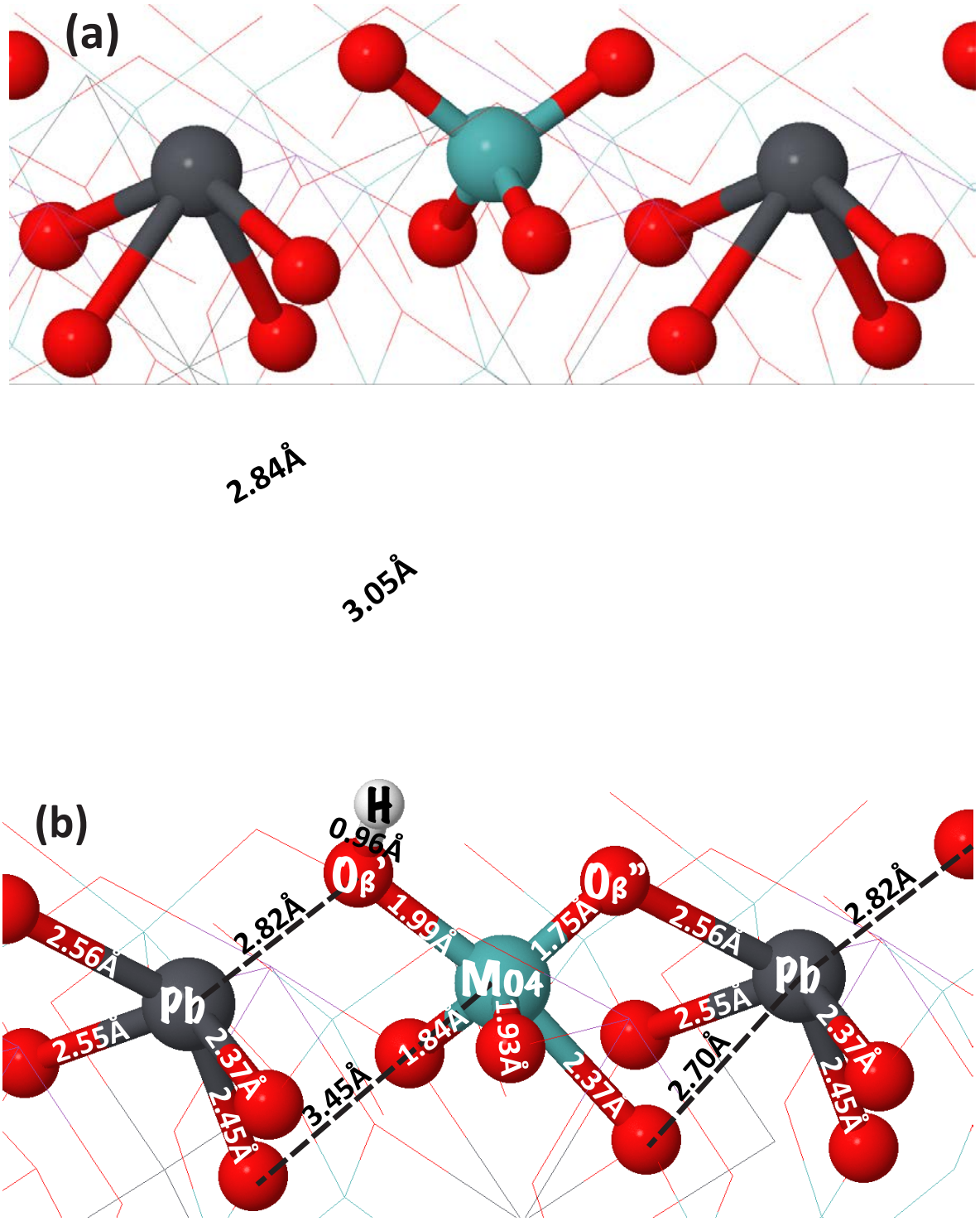

Fig. 6 (a) Side view of both a Pb row (top) and a Bi row (bottom) on the fully oxidized surface of $Bi_2Pb_5Mo_8O_{32}$ showing the four different types of surface oxygen atoms (b) Pb row after one hydrogen addition to O_β'. Relevant distances in Å are indicated on the bond or with a dashed line between atoms.

3.3.4 Molybdenum Trioxide

Molybdenum trioxide, MoO_3, has a completely different structure than the pure and distorted scheelite mixed-metal oxides discussed above. In the bulk, molybdenum atoms have an octahedral geometry, with two doubly bound oxygen atoms, two singly bound oxygen atoms, and two loosely coordinated oxygen atoms. This remains true for the fully oxidized surface (Fig. 7a), which is terminated by pure doubly bonded oxygen atoms protruding out of the surface (O_α). The other doubly bonded oxygen (O_β) is in the surface plane and is loosely coordinated to neighboring molybdenum and thus electronically perturbed by it. Each surface molybdenum atom is loosely coordinated to a sixth oxygen underneath it (O_δ) that is doubly bonded to the molybdenum one layer below the surface. These equivalent 6-coordinate molybdenum surface units are located at the vertices of a ~3.9 Å square grid.

As shown in Fig. 7b, upon hydrogen addition to the protruding O_α, the molybdenum atom it is bound to sinks into the surface of the catalyst, resulting in a 0.24 Å shorter bond to the O_δ beneath the surface. This action leaves each molybdenum atom with a planar double bond to O_β, and partial or single bonds to the five remaining surrounding oxygen atoms, including the O_α where the hydrogen was added. The energy for hydrogen addition is -58.2 kcal/mol (see Table 2), the same as the energy for hydrogen addition to O_β of $Bi_2Mo_3O_{12}$. However, the former has a much more negative HAE when the surface is frozen and only the hydroxyl group is allowed to relax (bracketed numbers in Table 2). Therefore, the O_α on the 6-coordinate molybdenum of MoO_3 is the better intrinsic hydrogen addition site, but the conformational flexibility in $Bi_2Mo_3O_{12}$ allows that O_β to achieve a similar HAE.

In Fig. 7c, we present the optimized geometry after hydrogen addition to O_β, which has the lowest HAE by 5 kcal/mol of any oxygen we tested. However, since we are using a square unit

cell containing a 2x2 grid of O_β atoms, some of this ability to rearrange and thus attain a low energy is an artifact of the periodic boundary conditions. The actual HAE for a single hydrogen atom addition at this position if there were no periodicity is likely less negative than the value we calculate. Indeed, the HAE value for hydrogen addition when only the hydroxyl is allowed to relax is less negative than that of any of the other surface oxygen atoms examined, indicating that surface relaxation is especially important in the case of the MoO_3 O_β. Unfortunately, we are unable to determine what fraction of this relaxation energy is due to the artificial periodic boundary conditions, and therefore cannot subtract out this component to obtain the actual value. However, O_β will not be accessible to propene when only the (010) surface of MoO_3 is exposed, since propene is too large to fit between the O_α atoms that protrude from the surface without experiencing large repulsive interactions with the aforementioned oxygen atoms. Therefore, because it should not be physically relevant and our calculations cannot accurately predict its HAE, we do not consider propene reaction at O_β, only at O_α.

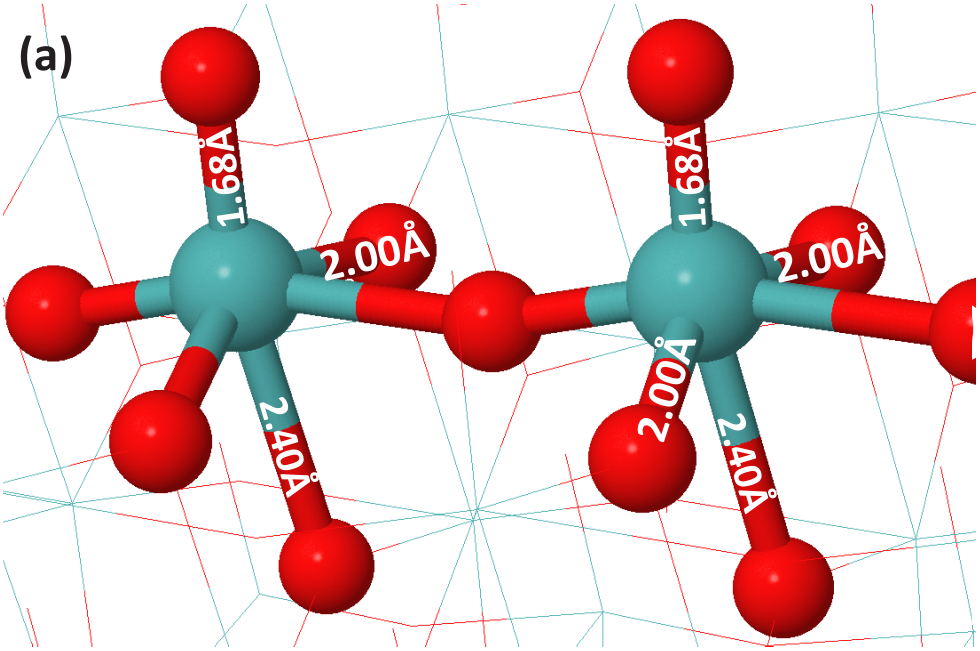

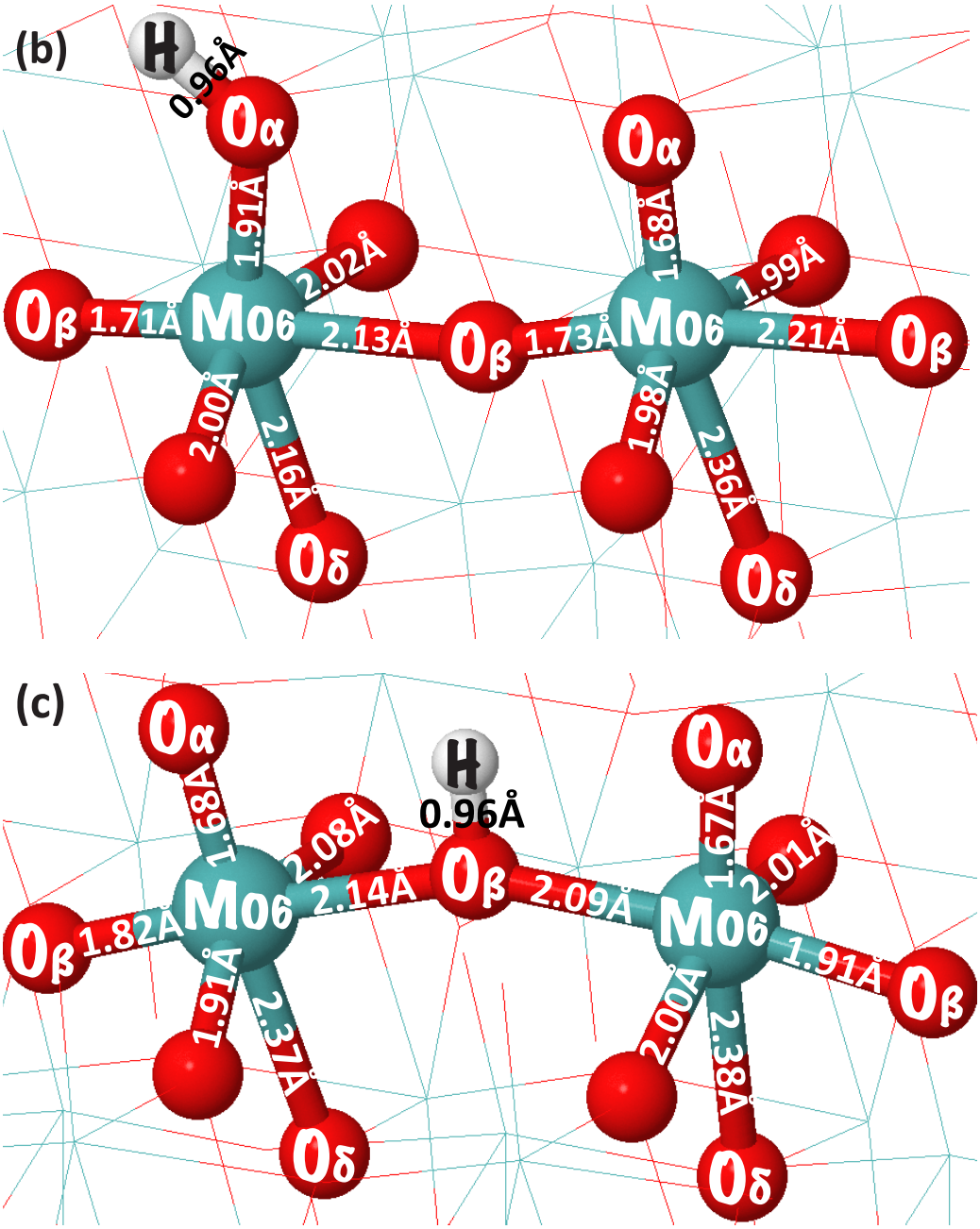

Fig. 7 (a) Side view of the fully oxidized surface of MoO_3. (b) The same view after hydrogen addition to one of the equivalent O_α atoms. (c) The same view after hydrogen addition to one of the equivalent O_β atoms. Relevant distances in Å are indicated on the bond

3.4 Molecular Orbital Analysis

In this section representative molybdenum cluster calculations are used to develop a deeper understanding for why oxo groups on 5-coordinate molybdenum atoms have a more negative

energy for hydrogen addition than do 4-coordinate molybdenum atoms. For this analysis a 4-coordinate molybdenum unit $MoO_2(OH)_2$ is allowed to interact with a molecule of dimethyl ether (DME = $O(CH_3)_2$) to ultimately form a 5-coordinate unit $MoO_2(OH)_2$-$O(CH_3)_2$. The oxygen atom of DME, O_δ, is oriented so that it interacts with the molybdenum via its oxygen atom as shown in Fig. 8. The orientation of DME relative to the $MoO_2(OH)_2$ fragment is not constrained geometrically and is defined by the lowest energy configuration. Interaction of DME with $MoO_2(OH)_2$ results in two distinct molybdenyl oxo groups, one cis to the DME (O_{Cis}) and one *trans* to the DME (O_{Tr}), as noted in Fig. 9. The 4-coordinate cluster is representative of the molybdenum coordination environment in $PbMoO_4$, while the 5-coordinate cluster is representative of the molybdenum coordination environment in $Bi_2Mo_3O_{12}$.

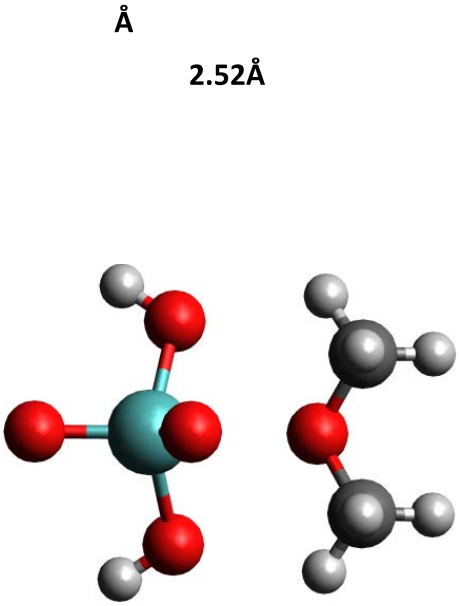

Fig. 8 Two views (top: xy plane, bottom: xz plane) of the 5-coordinate $MoO_2(OH)_2$-$O(CH_3)_2$ model cluster used to analyze the frontier molecular orbitals. The 4-coordinate cluster is the molybdate unit optimized without the $O(CH_3)_2$ molecule.

Fig. 9 shows how the system energy changes as the DME moves from infinity towards the 4-coordinate molybdate cluster to create a 5-coordinate molybdate cluster, both for the cases of no

addition and addition of a hydrogen atom to O_{Tr}. As can be seen in Fig. 8, the length of a molybdenum-oxygen double bond is ~1.7 Å and that of a single bond ~1.9 Å. Fig. 9 therefore depicts the range of Mo-O_δ distances between a full single bond and no interaction. For distances greater than ~ 3.0 Å, the relative energies of the cluster before and after hydrogen addition are similar, and in both cases the energy decrease relative to the 4-coordinate cluster is mainly due to non-specific van der Waals type interactions between the molybdate unit and the DME. However, for distances less than ~ 3.0Å, we observe mixing between orbitals centered on the molybdate unit and orbitals centered on O_δ of DME, indicative of a specific interaction between the two (see below).

For the $MoO_2(OH)_2$-$O(CH_3)_2$ cluster with Mo-O_δ distances < 3.0Å, repulsion between electrons on O_δ and electrons on the $MoO_2(OH)_2$ unit results in the energy profile reaching a minimum and then increasing sharply. However, after hydrogen addition to the O_{Tr} oxygen atom of the $MoO_2(OH)_2$-$O(CH_3)_2$ cluster, interaction between O_δ and the molybdate is favorable, resulting in a 11 kcal/mol decrease in the relative energy as the Mo-O_δ distance decreases from 3.0 Å to 2.2 Å. Note that the curves in Fig. 9 are shown on the same scale for ease of comparison, but on an absolute energy scale would be offset by the HAE of the reference 4-coordinate molybdate cluster, -39.6 kcal/mol. Therefore, as indicated on the plot, the energy difference between the two curves is the ΔHAE relative to the reference compound. By considering the ΔHAE, it is clear that the HAE decreases monotonically from -39.6 kcal/mol with decreasing Mo-O_δ distance, since the cluster after hydrogen addition is always more stabilized by the presence of DME than is the cluster before hydrogen addition.

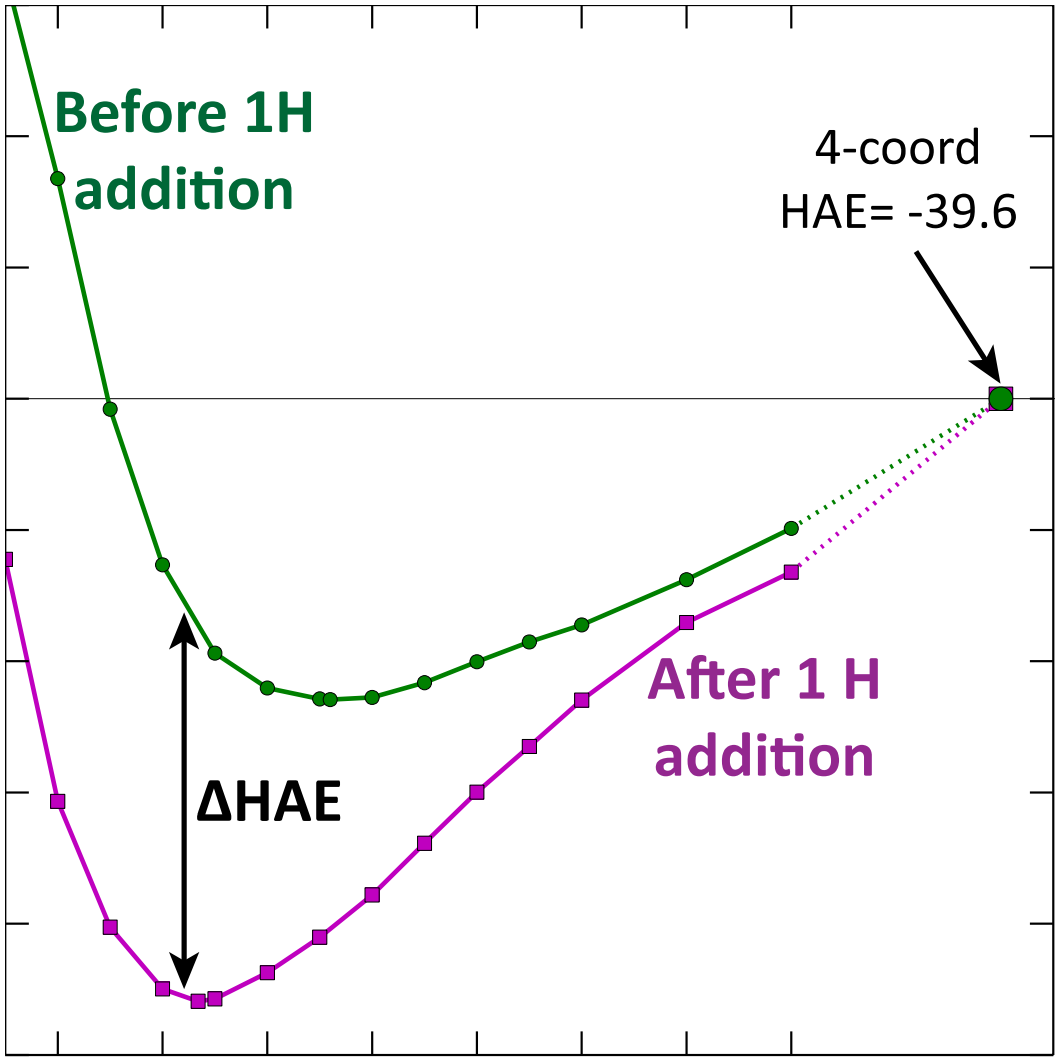

Fig. 9 Energy for the 5-coordinate molybdate cluster both before and after hydrogen addition as a function of Mo-O_δ distance. For each case, the plotted energy is relative to the energy of the 4-coordinate molybdate cluster before or after hydrogen addition, respectively, plus the energy of DME.

To further elucidate why the approach of DME to Mo has different effects on the cluster before and after hydrogen addition, we applied the Born-Haber cycle approach summarized in Fig. 10a and explained in greater detail in our previous work.[22] In this approach, the HAE can be

represented as the sum of three components: (1) the energy (E_{Geom}) to move the atoms from their initial positions prior to hydrogen addition to their final positions after addition, (2) the energy (E_{Hyb}) to rehybridize the molybdenum-oxygen double bond from the singlet spin state to the triplet spin state with the atom positions held constant in their final positions, and (3) the energy (E_{OH}) to bring a hydrogen radical from infinity and add it to the cluster, which already has the atoms in their final positions, thereby forming a spin-doublet molybdenum hydroxyl group. Fig. 10b illustrates how the values of these three components change with Mo-O_δ distance. The component with the largest change upon coordination with DME is E_{Hyb}, followed by E_{Geom}, and finally E_{OH}.

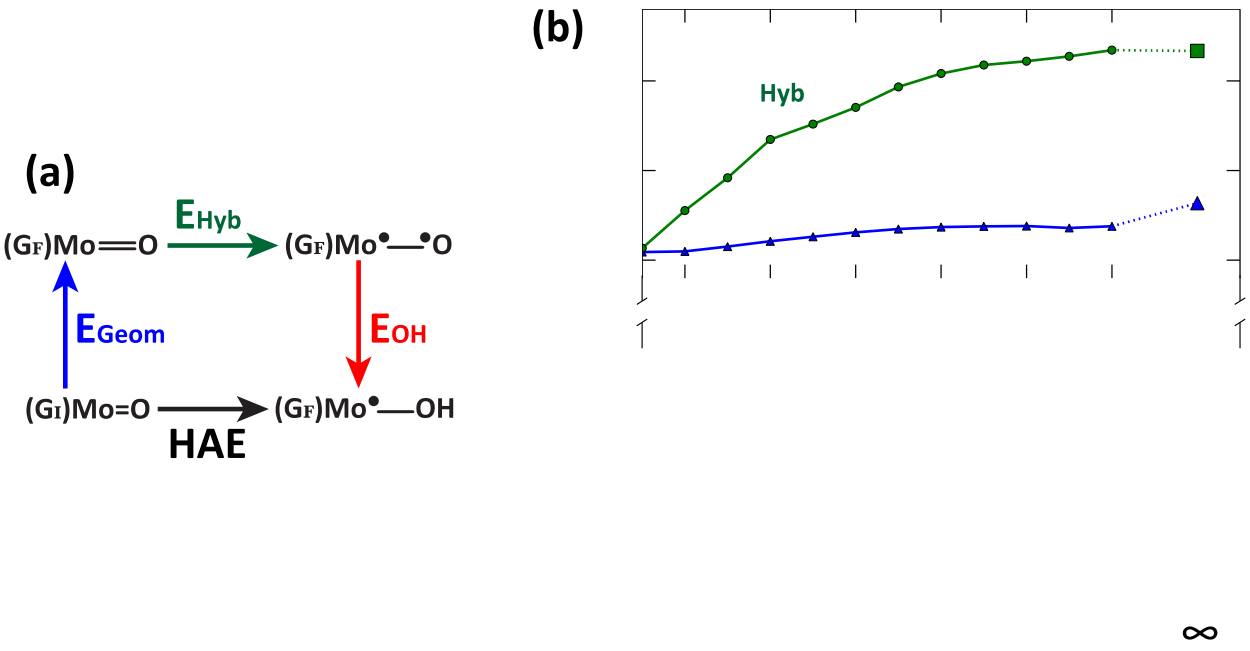

Fig. 10 (a) HAE decomposition into components E_{Geom}, E_{Hyb}, and E_{OH}. (b) Plot of these components versus Mo-O_δ distance.

E_{Hyb}, is directly related to the energy difference between the relevant highest occupied molecular orbital (HOMO) and the relevant lowest unoccupied molecular orbital (LUMO). In Fig. 11, we show the energy of the frontier molecular orbitals as a function of Mo-O_δ distance. There

are 5 specific molecular orbitals that are important, labeled A, B', B" C, and D. Electron density plots for these 5 types are shown on the right of Fig. 11. Molecular orbital type A is comprised mainly of O_{Tr} p_y and O_{Cis} p_x lone pair orbitals and is the HOMO for the 4-coordinate molybdate cluster. Molecular orbital type C is comprised mainly of O_δ p_x and is the HOMO for DME. Molecular orbital type B' and type B" are both hybrid molecular orbitals that result from mixing types A and C as the Mo-O_δ distance decreases. Note that, at d=2.9Å (see Fig. 11), B' and B" appear very similar, but they diverge in both character and energy as d decreases. Type B' always has more type A character and is always higher in energy than type B", which has more type C character. Type B' is therefore the HOMO for the 5-coordinate cluster at Mo-O_δ distances $\leq$2.9 Å and is higher in energy than the molybdate HOMO (A) because of orbital mixing with the p orbital on the approaching O_δ. Finally, orbital type D is a π anti-bonding orbital between Mo d_{xz} and O_{Tr} p_z and is the LUMO for both 4- and 5-coordinate molybdate clusters. Fig. 11 identifies the HOMO-LUMO energy differences for two relevant species: the isolated 4-coordinate molybdate (2.88 eV) and a 5-coordinate molybdate with Mo-O_δ distance 2.27 Å (2.47 eV).

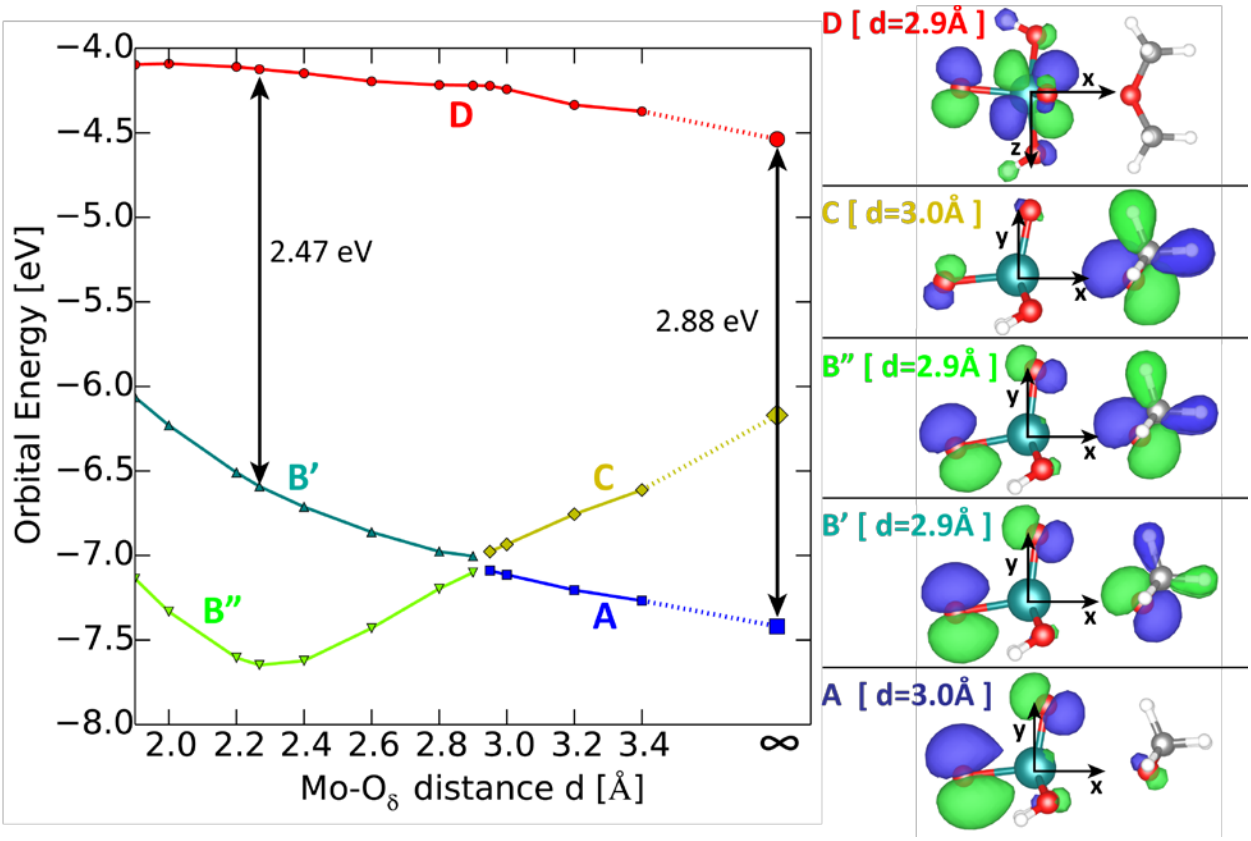

Fig. 11 Highest occupied molecular orbital (HOMO) and lowest unoccupied molecular orbital (LUMO) energies as a function of the distance from the oxygen atom in DME (O_δ) to the molybdenum atom in the $MoO_2(OH)_2$ cluster. These calculations are for geometries optimized after hydrogen addition to the oxygen *trans* to the DME (O_{Tr}), then frozen in place, the hydrogen removed and the orbital energies calculated in the singlet state. The orbital pictures shown on the right are for d = 2.27 Å. d = ∞ is for the optimized 4-coordinate $MoO_2(OH)_2$ cluster.

It is evident from Fig. 11 that orbital mixing between the higher energy O_δ p_x (C) molecular orbital and the lower energy O_{Tr} p_y plus O_{Cis} p_x (A) molecular orbital results in two combined molecular orbitals (B' and B") that have intermediate energy. Importantly, the combined orbital B' that is the HOMO for the 5-coordinate cluster (with d ≤2.9 Å) is higher in energy than that of the unmixed orbital (A) that is the HOMO for the 4-coordinate cluster, and increases in energy with decreasing Mo-O_δ distance. The LUMO also increases slightly in energy as DME is brought towards the molybdate, but the influence is much weaker than for the HOMO, and therefore the HOMO-LUMO gap decreases monotonically with decreasing distance. The HOMO-LUMO gap

is directly related to E_{Hyb}, which, as shown in Fig. 10, is the component of the HAE that changes most significantly with Mo-O_δ distance. Therefore, addition of a fifth oxygen to the molybdate coordination sphere (Mo-O_δ $\leq$2.9 Å) results in a more negative HAE because of orbital mixing between the molybdate cluster and the additional oxygen.

We further note that the same orbital mixing effect is observed in the cluster before hydrogen addition. Again, the mixed type B' cluster HOMO increases in energy with decreasing distance. In doing so, it raises the energy of the cluster itself. This explains why the interaction energy between DME and the molybdate prior to hydrogen addition reaches a minimum and then increases in energy as DME enters the coordination sphere (see Fig. 9).

Up to this point in the discussion of the cluster calculations, we have only considered hydrogen addition to O_{Tr}, the oxygen that is *trans* to the DME. For hydrogen addition to O_{Cis} with d=2.392Å (the optimal Mo-O_δ distance after H addition to O_{Cis}), E_{Geom} = 1.06 eV, E_{Hyb} = 2.28 eV, and E_{OH} = -4.92 eV. These sum to give an HAE of -36.4 kcal/mol, which is slightly less negative than the HAE for the 4-coordinate molybdate cluster (-39.6 kcal/mol), and significantly less negative than the HAE for addition to O_{Tr} at the same Mo-O_δ distance (-50.4 kcal/mol). During H addition to either O_{Tr} or O_{Cis}, an electron is promoted from the type B' HOMO to the type D LUMO. However, when H is added to O_{Tr} the Mo=O_{Tr} bond lengthens (1.694Å $\rightarrow$ 1.930Å), while when H is added to O_{Cis}, the Mo=O_{Cis} bond lengthens (1.699Å $\rightarrow$ 1.925Å). Lengthening either bond increases the energy of the type B' HOMO and decreases the energy of the type D LUMO, however to different extents for O_{Tr} and O_{Cis}. As shown in Fig. S3 for a fixed Mo-O_δ distance d=2.392Å, lengthening the Mo=O_{Tr} bond to its optimal length after H addition results in an overall lower HOMO-LUMO gap than does lengthening the Mo-O_{Cis} bond to its optimal length after H addition. This is due to a larger decrease in the LUMO energy for stretching the Mo=O_{Tr} bond,

which has more π anti-bonding overlap between the Mo d_{xz} orbital and the O_{Tr} p_z orbital than between the Mo d_{xz} orbital and the O_{Cis} p_z orbital (see Fig. 11 type D orbital depiction). Since the E_{Hyb} is calculated after Mo=O bond lengthening, the E_{Hyb} of addition to O_{Tr} is lower than the E_{Hyb} of addition to O_{Cis}. In addition, as also shown in Fig. S3, the type B' HOMO is higher in energy after lengthening O_{Cis} its final length than after lengthening O_{Tr} to its final length. Since the H electron goes into this type B' orbital in order to form the O-H bond (after one electron is promoted from the type B' HOMO to the type D LUMO in the rehybridization step), a higher energy type B' orbital results in a less favorable O-H bond. Therefore, the less negative E_{OH} and more positive E_{Hyb} of addition to O_{Cis} relative to addition to O_{Tr} are both due to the different effects on the orbital energies upon stretching Mo=O_{Cis} and stretching Mo=O_{Tr}, and sum to result in a less negative HAE.

By extracting the components of the HAE for hydrogen addition to O_{Cis}, we determined that E_{Hyb} is 2.28 eV in this case, which is higher than the value for the 4-coordinate molybdate, 2.17 eV. This high value of E_{Hyb} is a result of promotion of an electron from the mixed type B' HOMO to a LUMO that not only has significant π anti-bonding between Mo d_{xz} and O_{Tr} p_z, but that also has substantial π anti-bonding between Mo d_{xz} and O_{Cis} p_z.

We have also considered a 6-coordinate molybdate cluster where the primary $MoO_2(OH)_2$ unit is coordinated with two DME molecules, one on each side such that the doubly bound oxygen atoms are essentially equivalent. The HAE on the 6-coordinate cluster optimized before and after hydrogen addition is -49.8 kcal/mol, which is close to the HAE for a 5-coordinate cluster optimized before and after hydrogen addition (-51.1 kcal/mol). This result is consistent with findings discussed in the previous paragraph, namely that adding an oxygen donor to the coordination sphere in a position *trans* to a molybdenyl oxo renders the HAE on that oxo significantly more

negative, but has little impact on the HAE of the oxo that is cis to the additional oxygen. Therefore, since both molybdenyl oxo groups in the 6-coordinate cluster have donor oxygen atoms in a *trans* positions, both exhibit low HAE values similar to that of O_{Tr} in the 5-coordinate cluster.

The insights gained from the cluster calculations help to explain what is observed before and after hydrogen addition to the surface of bulk molybates presented in Section 3.4. As mentioned there, upon hydrogen addition, molybdenum always relaxes towards the closest oxygen that is *trans* to the location of the oxygen atom to which the hydrogen was added. This change can be understand in the context of the cluster calculations by recalling that the presence of an additional oxygen atom in the coordination sphere around Mo is energetically unfavorable before hydrogen addition, but energetically favorable after hydrogen addition.

Because of the energetic penalty for introducing an additional oxygen atom into the coordination sphere of molybdenum, bulk mixed metal molybdates would be expected to always form low-energy 4-coordinate MoO_4^{2-} units spaced between charge compensating cations. Indeed, most mixed metal molybdates, including $PbMoO_4$, $La_2Mo_3O_{12}$, $Ce_2Mo_3O_{12}$ and $Eu_2Mo_3O_{12}$, exhibit only 4-coordinate molybdenum atoms, even when vacancies are present that distort the scheelite structure. Since these materials have molybdenum in its most favorable coordination environment, they will have much higher HAE values than materials that have additional oxygen atoms in the molybdenum coordination sphere. In all of the structures listed above, the next closest oxygen atom to any molybdenum atom (after its 4 coordinated oxygen atoms) is at least 2.9 Å away, and therefore would require significant structural distortion upon hydrogen addition in order to achieve a substantial decrease in HAE. In the case of $PbMoO_4$, such structural distortion must not be energetically feasible, since, in the optimized geometry after hydrogen addition (Fig. 4b), the molybdenum is still 4-coordinate and the HAE is only -44.0 kcal/mol. However, in the case of

$Bi_2Pb_5Mo_8O_{32}$, the vacancies that result from replacing Pb^{2+} with Bi^{3+} allow for more distortion, and therefore, after addition to O_β', the molybdenum is able to coordinate slightly with a bulk oxygen, thereby making the HAE more negative by 4 kcal/mol relative to $PbMoO_4$ O_β.

By contrast, $Bi_2Mo_3O_{12}$ has exclusively 5-coordinate molybdenum units in the bulk crystal, two thirds of which remain 5-coordinate on the (010) surface. We also note that β-$Bi_2Mo_2O_9$ and γ-Bi_2MoO_6, which have propene oxidation activities similar to that of α-$Bi_2Mo_3O_{12}$,[4,5] have molybdenum atoms in the bulk that have more than 4 oxygen atoms in their coordination sphere. It is less obvious what surface structures these materials present, but at least some of the surface molybdenum atoms are likely to retain their high coordination number. As shown by the molecular orbital analysis presented above, locating an additional oxygen atom *trans* to the oxygen to which the hydrogen atom is added and close to the molybdenum atom allows for orbital mixing that increases the energy of the HOMO. This results in more highly coordinated Mo cations that are higher in energy, but also have a more negative HAE. As mentioned above, 5- and 6-coordinate molybdenum clusters have comparable HAE values for the oxo group(s) *trans* to a coordinated oxygen atom, therefore metal oxide materials with more highly coordinated molybdenum atoms should exhibit similar HAE values that are higher than those of materials with only 4-coordinate molybdenum atoms. We note that, indeed, $Bi_2Mo_3O_{12}$ O_β, which is *trans* to an oxygen on a 5-coordinate Mo, and MoO_3 O_α, which is *trans* to a oxygen on a 6-coordinate Mo, have identical HAEs. Addition to O_α of $Bi_2Mo_3O_{12}$ results in a quasi-6-coordinate Mo after optimization, but the Mo distance from the oxygen *trans* to O_α is significantly further than in the former cases, resulting in a somewhat less favorable HAE.

From this analysis, we discover that an important role of bismuth in making bismuth molybdates active catalysts for propene oxidation and ammoxidation is to force Mo^{6+} cations into

a higher energy, higher coordination configuration, thereby facilitating acceptance of a hydrogen atom from propene by a Mo=O group.

3.5 Reaction of Propene

In this section, we consider the effect of propene adsorption to an oxidized surface and the reaction energy to move one hydrogen atom from the methyl group of adsorbed propene to the most active surface oxygen atom. In every case, the physisorbed propene is oriented such that one of the hydrogen atoms on the methyl group is pointed toward the oxygen atom that will accept the H atom resulting from the cleavage of a C-H bond. For all materials, the final distance between the H and O atom that will abstract it is in the range of 2.2-2.5 Å. Reference will be made to the ΔE_{ads} values listed in Table 4 and to the energy levels depicted in Fig. 12. In the discussion below, the initial state for each material is a bare oxidized surface and propene in the gas phase (the zero energy reference point) and the final state is the surface with one hydrogen atom added to the oxygen atom indicated in Table 4 and a physisorbed allyl radical.

3.5.1 Propene Adsorption

As mentioned in Section 3.3.1, bismuth cations on the surface of $Bi_2Mo_3O_{12}$ are under-coordinated compared to their desired coordination in the bulk. Because of this, they are good sites for adsorbing gas-phase molecules that can donate electron density via a dative type bond to Bi^{3+}. From DFT calculation results, we have recently reported that surface bismuth cations on the (010) surface of $Bi_2Mo_3O_{12}$ can favorably adsorb both ammonia, via σ-donation from the lone pair on nitrogen, and propene, via donation of π electron density from the carbon-carbon double bond.[6,17] Additionally, this is a good adsorption site because the bismuth cations are close to the surface and there is space on either side where the methyl group of propene can sit without encountering repulsive interactions with surface oxygen anions. The calculated energy for propene

adsorption at this site is -11.5 kcal/mol and the distance between the bismuth cation and the midpoint of the carbon-carbon double bond is 3.33 Å, with the double bond situated directly above the bismuth cation. Since the acceptor 6p orbitals on bismuth are large and diffuse, propene can be situated anywhere within a ~2x2 Å square parallel to the surface at a distance of 3-3.5Å above Bi^{3+} and maintain a $\Delta E_{ads,C3H6} < -10$ kcal/mol. As a consequence, the entropy loss upon adsorption is not as large as it would be for a more localized mode of adsorption.

Similarly, propene can adsorb above Pb^{2+} on the surface of $PbMoO_4$, since these cations are also under-coordinated compared to the environment in the bulk. However, these sites are less favorable for propene adsorption than the Bi^{3+} sites in $Bi_2Mo_3O_{12}$ by 4 kcal/mol (see Table 4). This difference is attributable to the fact that the lead cations in lead molybdate are not as close to the surface as the bismuth cations are in bismuth molybdate, and the former material has more surface oxygen anions at shorter distances that interact repulsively with the adsorbed propene. Additionally, the lower charge on the lead cations results in them being weaker Lewis acids than bismuth cations.

The mixed bismuth/lead molybdate has stronger propene adsorption sites than the pure lead molybdate, with adsorption energies comparable to those on $Bi_2Mo_3O_{12}$ (see Table 4). For this material, the propene adsorbs over surface Bi^{3+} cations one row over from the most active O_β', which is in the Pb^{2+} row. This orientation is very similar to the orientation in $Bi_2Mo_3O_{12}$ and is a favorable geometry for hydrogen abstraction.

Finally, propene adsorption on molybdenum trioxide is not favorable, as is obvious from the very low calculated energy of adsorption of -1.8 kcal/mol. This is because the surface of MoO_3 is covered by oxygen O_α anions, whose lone pair will have repulsive interactions with propene. Propene is too large (approximately 3 Å x 4 Å) to fit in the spaces of the 3.9 Å x 3.9 Å surface O_α

atom grid, further reducing the ability of propene to adsorb effectively. Unlike the scheelite mixed-metal molybdates, MoO_3 does not have under-coordinated surface cations with which propene can interact favorably.

3.5.2 Hydrogen Abstraction from Propene

Fig. 12 displays the relevant energy parameters for the most active surface oxygen on the four different metal oxide surfaces studied. The energy of the final state, allyl radical adsorbed over a surface with one hydrogen atom added to a Mo=O group, relative to the zero energy reference state of bare oxidized surface with propene in the gas phase is a measure of the ability of the catalyst to activate propene. As discussed in the Introduction, the energy of this final state is a lower bound on the apparent activation energy. For $Bi_2Mo_3O_{12}$, the only material for which we have calculated the full reaction barrier, the transition state is only 7.6 kcal/mol above the final state.[17,38] Given what we know from the Born-Haber cycle decomposition of the transition state energy,[22] we expect that the combination of HAE and propene adsorption captures the major components of the transition state, and therefore we expect that the other materials have actual transition state energies that are similarly close in energy to the final state. However, regardless of the difference between the two, the transition state cannot be lower in energy than the final state.

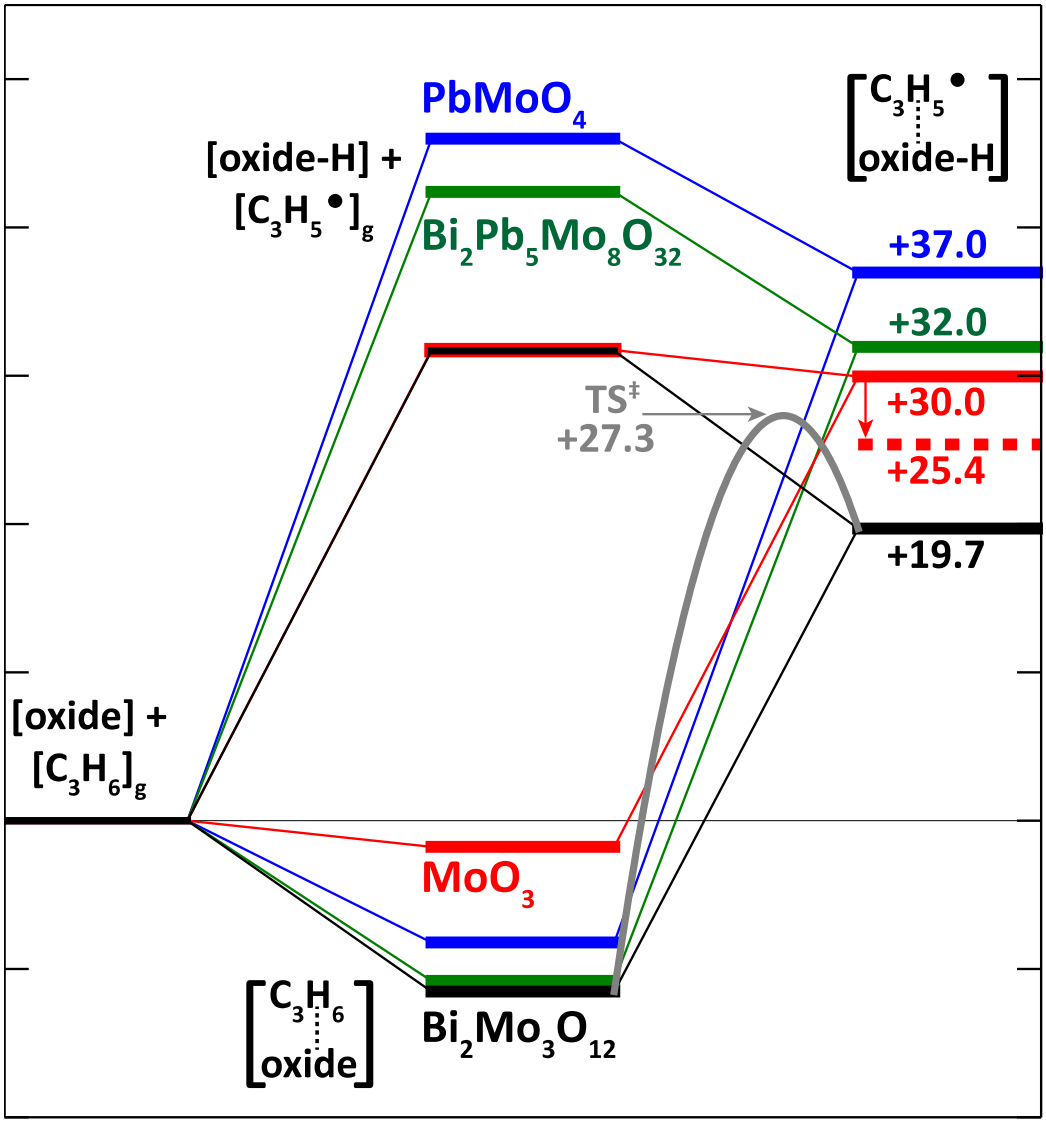

Fig. 12 Relevant energy values for first hydrogen abstraction from propene. Normalization point for all materials is a bare oxidized surface plus propene in the gas phase. Full reaction barrier through the transition state shown only for $Bi_2Mo_3O_{12}$. The two final state values for MoO_3 are shown, one for $\Delta E_{ads,C3H5}$ = $\Delta E_{ads,C3H6}$ (solid line) and one for calculated $\Delta E_{ads,C3H5}$ (dashed line). The appropriate comparison between materials is the energy of the final state indicated with a solid line.

Material & Surface Oxygen	**$\Delta E_{ads,C3H6}$ on oxidized surface [kcal/mol]**	**$\Delta E_{ads,C3H5}$ on 1-H surface [kcal/mol]**
$Bi_2Mo_3O_{12}$ [O_β]	-11.5	-12.0
$PbMoO_4$ [O_β]	-8.2	-9.0
$Bi_2Pb_5Mo_8O_{32}$ [O_β']	-10.3	-10.4
MoO_3 [O_α]	-1.8	-6.4

Table 4. Propene adsorption energy on an oxidized surface ($\Delta E_{ads,C3H6}$) and allyl adsorption energy on a one hydrogen added surface ($\Delta E_{ads,C3H5}$) for each of the four tested materials.

Fig. 12 demonstrates that $Bi_2Mo_3O_{12}$ is a good catalyst for propene activation because it has a low energy for propene adsorption near the most active oxygen, which itself has a low HAE. Together, these effects combine to give a final state energy of 19.7 kcal/mol, the lowest of any material examined in this study. Additionally, as is apparent from Fig. 2, propene adsorbed to a surface bismuth cation is within reach of three O_β atoms, and this configuration enhances the probability of hydrogen abstraction. Moreover, the character of the Bi orbitals allows for favorable dative interaction between propene and bismuth to be partially maintained in the transition state, which should help stabilize the allyl radical as it forms.[17]

The next lowest final state energy is for MoO_3. Most studies have found MoO_3 to be inactive;[36,37] however, there have been some reports of measurable propene conversion to acrolein at higher temperatures.[59] One study has investigated the role of the exposed surface plane for epitaxial MoO_3 deposited on graphene, and observed that the higher the concentration of the lowest energy (010) plane, the lower the production of acrolein.[59] Our results are consistent with these conflicting reports. For a fully oxidized surface exposing only the (010) surface plane, we would not expect significant propene oxidation because the final state energy for hydrogen abstraction by O_α is too high (see Fig. 12 and additional details below). However, higher energy surface planes may expose a few of the O_β atoms that are inaccessible on the (010) surface, and these O_β atoms

may be even more active for hydrogen abstraction than the O_α atoms. Additionally, if the catalyst is not fully oxidized under working conditions, propene may be able to adsorb favorably at any under-coordinated surface molybdenum sites and then undergo reaction. Both of these influences could lead to some measurable propene oxidation activity. However, under O_2-rich conditions, the surface of MoO_3 is expected to remain oxidized, with few to no propene adsorption sites and, therefore, to be lower in activity relative to $Bi_2Mo_3O_{12}$.

While the O_β sites on MoO_3 remain inaccessible to gas phase propene, the O_α sites have a favorable HAE equal to that of O_β sites on $Bi_2Mo_3O_{12}$. The 9 kcal/mol difference in propene adsorption energy between these two materials with equal HAE should translate to a MoO_3 final state with an energy 9 kcal/mol above that of $Bi_2Mo_3O_{12}$. However, as is clear from Table 4, the adsorption of allyl radical is 5 kcal/mol lower in energy than the adsorption of propene. The stronger allyl adsorption on MoO_3 is due to coordination with a surface O_α, resulting in stabilization of the polarizable allyl radical by oxygen. This phenomenon is not observed for the other materials, which have allyl adsorption energies approximately equal to that of propene and for which insertion of the allyl radical into a Mo=O bond occurs as a separate step.[17,21] Since the allyl is formed in the transition state, this additional allyl stabilization only occurs after the transition state, making it irrelevant to the reaction barrier for hydrogen abstraction from propene. Therefore, the final state for MoO_3 that is more comparable to that for the other oxides is for an allyl radical adsorption energy approximately equal to that of propene. Making this adjustment leads to final-state energy of +30.0 kcal/mol for MoO_3 (the solid line in Fig. 12). Therefore, MoO_3 is expected to be considerably less active than $Bi_2Mo_3O_{12}$, since the lower bound on its transition-state energy is 3 kcal/mol higher than the calculated transition-state energy for $Bi_2Mo_3O_{12}$, and the actual transition state energy will be even higher. Thus, MoO_3 is a poor catalyst for the activation

of propene not because it has inactive oxygen atoms, but because it does not adsorb propene so that it can interact with the active oxygen atoms.

$PbMoO_4$ is clearly inactive for propene activation because of both unfavorable hydrogen addition sites and moderately weak propene adsorption sites. The calculated final state energy of +37.5 kcal/mol (Fig. 12) is consistent with experimental reports that this material does not catalyze propene oxidation.[29]

Finally, the mixed bismuth lead molybdate shows a final state energy between those for pure lead molybdate and pure bismuth molybdate. The experimental results show an activity closer to $Bi_2Mo_3O_{12}$ than we predict from our DFT calculations;[27] however, it is not known what the bismuth to lead ratio is on the surface of a mixed molybdate or where the vacancies occur and if they are distributed randomly or in an ordered manner; therefore, we do not know how close our model is to the observed structure. Nevertheless, this material allows us to explore the effect of introducing vacancies, and we do observe the correct trend moving from $PbMoO_4$ to $Bi_2Pb_5Mo_8O_{32}$.

Our analysis shows that $Bi_2Pb_5Mo_8O_{32}$ has both stronger propene adsorption sites and more negative values of the HAE than $PbMoO_4$. As mentioned above, these outcomes are both consequences of the increased flexibility of the lattice that comes from introducing vacancies and Bi^{3+} cations, which are smaller than Pb^{2+} cations. The ability of the oxide to distort in order to achieve a more desirable coordination around molybdenum, as well as the distortion already present at the oxidized surface, explains why previous studies have associated high activity for propene activation to the presence of vacancies.[21,27,30] (see Introduction). The 3+ lanthanide scheelite molybdates, which have a vacancy ordering that is different from that in $Bi_2Mo_3O_{12}$, do not show activity for propene oxidation or ammoxidation. The reason is that the lanthanides lack

the stereochemically active lone pair that drives asymmetric coordination environments around bismuth and thereby enforce 5-coordinate geometries at molybdenum. Thus, despite containing cation vacancies, the lanthanide molybdates exhibit energetically preferred, but less catalytically active, 4-coordiante geometries at molybdenum. The results of the present study show why both bismuth and vacancies are required for an active molybdate-based catalyst, since together they induce higher molybdenum coordination in the oxidized state and provide the conformational flexibility required to further increase molybdenum coordination when a hydrogen atom is transferred to a Mo=O bond in the rate-limiting step of propene oxidation or ammoxidation.

4. Conclusions

Four different metal oxides containing molybdenum ($Bi_2Mo_3O_{12}$, $PbMoO_4$, $Bi_2Pb_5Mo_8O_{32}$, and MoO_3) have been analyzed with the objective of explaining their relative catalytic activity for propene oxidation and ammoxidation. This analysis is predicated on the assumption that the key step governing the ability of a catalyst to activate propene is the abstraction of a hydrogen atom from the methyl group of adsorbed propene to form a Mo-OH group and a physisorbed allyl radical. We find that a low reaction barrier for hydrogen atom abstraction requires a favorable site for propene adsorption that is proximate to a surface oxygen atom that has a low hydrogen adsorption energy (HAE).

Favorable propene adsorption occurs on under-coordinated surface metal cations via dative interaction between the π bond of propene and the metal cation. This interaction can be offset by repulsive interactions between propene and surface oxygen anions. Of the oxides examined, the strongest adsorption of propene occurs on Bi^{3+} present at the surface of $Bi_2Mo_3O_{12}$, because these cations are situated close to the surface and the nearest neighboring oxygen anions are far enough

away to have only a limited repulsive effect. Pb^{2+} in $PbMoO_4$ is not as favorable for propene adsorption as Bi^{3+}, since it is located slightly deeper in the surface and, hence, repulsive interactions with the neighboring oxygen anions play a larger role in reducing the adsorption energy. The least favorable energy of adsorption occurs for MoO_3 because this oxide has no under-coordinated cations at its surface, only protruding oxygen anions.

The second requirement for good catalyst activity is a surface oxygen atom with a high HAE. From observations of the geometric changes in the metal oxide surface upon hydrogen addition and additional detailed molecular orbital investigation of the influence of individual effects, we conclude that the most important structural property is a highly-coordinated molybdenum atom at the oxide surface. Molecular orbital analysis reveals that the presence of an oxygen atom *trans* to the oxo group to which a hydrogen is added increases the energy of the highest occupied molecular orbital, thereby reducing the energy required to rehybridize the molybdenum oxygen double bond from the singlet state to the triplet state. The energy for rehybridization is the energy component that has the strongest influence on the overall HAE, consistent with our previous work demonstrating that band gap correlates well with apparent activation energy.[22] The present investigation has revealed that greater than 4-coordinate molybdenum atoms are energetically disfavored, but are needed to achieve a low HAE.

In the absence of surface molybdenum atoms that are coordinated with more than four oxygen atoms, surface conformational flexibility can allow for a partial increase in oxygen coordination upon hydrogen addition. Evidence for this was observed in the case of $Bi_2Pb_5Mo_8O_{32}$, for which the surface has 4-coordinate molybdenum atoms that have a geometry very similar to that in $PbMoO_4$. However, the HAE for the lowest energy oxygen in the former structure is 4 kcal/mol more negative than that for the later structure. The introduction of

asymmetric Bi^{3+} in the surface layer of the parent structure and vacancies one layer below the surface give the mixed material the conformational flexibility to achieve favorable, higher molybdenum coordination after hydrogen addition. However, the molybdenum in $Bi_2Pb_5Mo_8O_{32}$ is not able to move as close to an additional oxygen atom in the final state as in the case of $Bi_2Mo_3O_{12}$. $Bi_2Pb_5Mo_8O_{32}$ also lacks the initial state destabilization that contributes to the more favorable value of HAE for $Bi_2Mo_3O_{12}$.

Finally, we have explored the ability of cations in metal molybdates to perturb the electronic properties of nearby Mo=O groups, a process that we had previously suggested was crucial for high activity.[19] Substitution of a surface Bi^{3+} in $Bi_2Mo_3O_{12}$ with Pb^{2+}+H^+, La^{3+} or Sb^{3+} demonstrated that other cations are able to have a similar electronic perturation effect as bismuth on the neighboring molybdenyl oxo. However, the presence of one of these cations only makes the HAE more negative by 3 kcal/mol relative to substitution of a surface Bi^{3+} in $Bi_2Mo_3O_{12}$ with B^{3+}, which does not have any interaction with the oxo. Therefore, the more critical role of bismuth is to force molybdenum into the 5-coordinate geometry that is significantly more active for abstracting a hydrogen from propene.

5. Acknowledgements.

Calculations presented in this work were conducted at the National Energy Research Scientific Computing Center (NERSC), which is supported by the Office of Basic Science of the U.S. Department of Energy under Contract No. DE-AC02-05CH11231. Additional calculations were performed at the University of California, Berkeley Molecular Graphics and Computation Facility, which is supported by NSF Grant CHE-0840505. Funding for this work was provided by the Director, Office of Science, Office of Basic Energy Sciences, and by the Division of Chemical

Sciences, Geosciences, and Biosciences of the U.S. Department of Energy at Lawrence Berkeley National Laboratory under Contract No. DE-AC02-05CH11231.

6. Supporting Information

The attached Supporting Information consists of three sections with additional information relevant to this work. The first section presents a diagram with the optimized geometries of the surface of $Bi_2Mo_3O_{12}$ after replacement of one Bi^{3+} with another cation (B^{3+}, La^{3+}, Pb^{2+} + H^+, and Sb^{3+}). The second section discusses the optimized geometries after H addition the other 3 surface oxygen atoms of $Bi_2Pb_5Mo_8O_{32}$ (only the geometry after addition to the lowest energy O_β' is discussed in the main text). The third section deals with the change in frontier orbital energies as the Mo=O bond lengthens for both O_{Cis} and O_{Tr}.

References

[1] Brazdil, J.F. *Ullmann's Encyclopedia of Industrial Chemistry*; Wiley-VCH: Weinheim, Germany, 2012.
[2] Grasselli, R.K. Fundamental Principles of Selective Heterogeneous Oxidation Catalysis. *Top. Catal.* **2002**, *21,* 79-88.
[3] Brazdil, J.F. Scheelite: a Versatile Structural Template for Selective Alkene Oxidation Catalysts. *Catal. Sci. Technol.* **2015**, *5*, 3452-3458.
[4] Grasselli, R.K.; Burrington, J.D.; Brazdil, J.F. Mechanistic Features of Selective Oxidation and Ammoxidation Catalysis. *Farad. Disc.* **1981**, *72*, 203-223.
[5] Matsuura, I.; Schut, R.; Hirakawa, K. The Surface Structure of the Active Bismuth Molybdate Catalyst. *J. Catal.* **1980**, *63*, 152-166.
[6] Licht, R.B.; Vogt, D.; Bell, A.T. The Mechanism and Kinetics of Propene Ammoxidation over α-Bismuth Molybdate. *J. Catal.* **2016**, *339*, 228-241.
[7] Callahan, J.L.; Grasselli, R.K.; Milberger, E.C.; Strecker, H.A. Oxidation and Ammoxidation of Propylene over Bismuth Molybdate Catalyst. *Ind. Eng. Chem. Prod. Res. Dev.* **1970**, *9*, 134-142.
[8] Wragg, R.D.; Ashmore, P.G.; Hockey, J.A. Heterogeneous Selective Ammoxidation over Bismuth Molybdate Catalysts. *J. Catal.* **1973**, *31*, 293-303.
[9] Kolchin, I.K.; Bobkov, S.S.; Margolia, L.Y. *Neftekhimiya* **1964**, *4*, 301-307.

[10] Adams, C.R.; Jennings, T.J. Investigation of the Mechanism of Catalytic Oxidation of Propylene to Acrolein and Acrylonitrile. *J. Catal.* **1963**, *2*, 63-68.
[11] Adams, C.R.; Jennings, T.J. Mechanism Studies of the Catalytic Oxidation of Propylene. *J. Catal.* **1964**, *3*, 549-558.
[12] McCain, C.C.; Gough, G.; Godin, G.W. Catalytic Oxidation of Propene. *Nature* **1963**, *198*, 989-990.
[13] Krenze, L.D.; Keulks, G.W. The Catalytic Oxidation of Propylene, VI. Mechanistic Studies Utilizing Isotopic Tracers. *J. Catal.* **1980**, *61*, 316-325.
[14] Burrington, J.D.; Kartisek, C.T.; Grasselli, R.K. Aspects of Selective Oxidation and Ammoxidation Mechanisms over Bismuth Molybdate Catalysts, 3. Subsituent Effects in the Selective Oxidation of Allylbenzenes. *J. Org. Chem.* **1981**, *46*, 1877-1882.
[15] Peacock, J.M.; Parker, A.J.; Ashmore, P.G.; Hockney, J.A. The Oxidation of Propene over Bismuth Oxide, Molybdenum Oxide, and Bismuth Molybdate Catalysts, IV. The Selective Oxidation of Propene. *J. Catal.* **1969**, *15*, 398-406.
[16] Keulks, G.W. The Mechanism of Oxygen Atom Incorporation into the Products of Propylene Oxidation over Bismuth Molybdate. *J. Catal.* **1970**, *19*, 232-235.

[17] Licht, R.B.; Bell, A.T. A DFT Investigation of the Mechanism of Propene Ammoxidation over α-Bismuth Molybdate. *In Press, ACS Catalysis, Nov. 2016.*
[18] Zhai, Z.; Getsoian, A.; Bell, A.T. The Kinetics of Selective Oxidation of Propene on Bismuth Vanadium Molybdenum Oxide Catalysts. *J. Catal*. **2013**, *308*, 25-36.
[19] Getsoian, A.; Shapovalov, V.; Bell, A.T. DFT+U Investigation of Propene Oxidation over Bismuth Molybdate: Active Sites, Reaction Intermediates, and the Role of Bismuth. *J. Phys. Chem. C* **2013**, *117*, 7123-7137.
[20] Pudar, S.; Oxgaard, J.; Goddard III, W.A. Mechanism of Selective Ammoxidation of Propene to Acrylonitrile on Bismuth Molybdates from Quantum Mechanical Calculations. *J. Phys. Chem. C* **2010**, *114*, 15678-15694.
[21] Burrington, J.D.; Kartisek, C.T.; Grasselli, R.K. Mechanism of Nitrogen Insertion in Ammoxidation Catalysis. *J. Catal*. **1983**, *81*, 489-498.
[22] Getsoian, A.; Zhai, Z.; Bell, A.T. Band-Gap Energy as a Descriptor of Catalytic Activity for Propene Oxidation over Mixed Metal Oxide Catalysts. *J. Am. Chem. Soc*. **2014**, *136*, 13684-13697.
[23] Snyder, T.P.; Hill, C.G. The Mechanism for the Partial Oxidation of Propylene over Bismuth Molybdate Catalysts. *Catal. Rev.* **1989**, *31*, 43-95.
[24] Hanna, T.A. The Role of Bismuth in the SOHIO Process. *Coord. Chem. Rev.* **2004**, *248*, 429-440.
[25] Brazdil, J.F.; Glaeser, L.C.; Grasselli, R.K. An Investigation of the Role of Bismuth and Defect Cation Vacancies in Selective Oxidation and Ammoxidation Catalysis. *J. Catal.* **1983**, *81*, 142-146.
[26] Theobald, F.; Laarif, A.; Hewat, A.W. Redetermination of the Crystal Structure of α-Bi_2O_3.3MoO_3 by Neutron Diffraction and the Catalytic Oxidation of Propene. *Mat. Res. Bull*. **1985**, *20*, 653-665.
[27] Sleight, A.W.; Linn, W.J. Olefin Oxidation over Oxide Catalysts with the Scheelite Structure. *Annals N.Y. Acad. Sci.* **1976**, 22-44.
[28] J. Leciejewicz, *Z. Kristallogr*. **1965**, *121,* 158.

[29] Aykan, K.; Sleight, A.W.; Rogers, D.B. Defect Control in Oxidation Catalysts. *J. Catal.* **1973**, *29*, 185-187

[30] Aykan, K.; Halvorson, D.; Sleight, A.W.; Rogers, D.B. Olefin Oxidation and Ammoxidation Studies over Molybdate, Tungstate, and Vanadate Catalysts Having Point Defects. *J. Catal.* **1974**, *35*, 401-406.

[31] Boulahya, K.; Parras, M.; Gonzalez-Calbet, J.M. Synthesis, Structure and Magnetic Characterization of a New Scheelite Related Compound: $Eu_2Mo_3O_{12}$ *Eur. J. Inorg. Chem.* **2005**, *5*, 967-970.

[32] Jeitschko, W. Crystal Structure of $La_2(MoO_4)_3$, a New Ordered Defect Scheelite Type. *Acta Cryst. B* **1973**, *29* (10), 2074-2081.

[33] Ueda, W.; Asakawa, K.; Chen, C.L.; Moro-Oka, Y.; Ikawa, T. Catalytic Properties of Tricomponent Metal Oxides Having the Scheelite Structure. *J. Catal.* **1986**, *101*, 360-368.

[34] Sleight, A.W.; Jeitchko, W. $Bi_3(FeO_4)(MoO_4)_2$ and $Bi_3(GaO_4)(MoO_4)_2$ – New Compounds with Scheelit Related Structures. *Mater. Res. Bull.* **1974**, *9*, 951-954.

[35] Swift, H.E.; Bozik, J.E.; Ondrey, J.A. Dehydrodimerization of Propylene Using Bismuth Oxide as the Oxidant. *J. Catal.* **1971**, *21*, 212-214.

[36] Grzybowska, B.; Haber, J.; Janas, J. Interaction of Allyl Iodide with Molybdate Catalyts for the Selective Oxidation of Hydrocarbons. *J. Catal.* **1977**, *49*, 150-163.

[37] Burrington, J.D.; Grasselli, R.K. Aspects of Selective Oxidation and Ammoxidation Mechanisms over Bismuth Molybdate Catalysts. *J. Catal.* **1979**, *59*, 79-99.

[38] Getsoian, A.; Bell, A.T. The Influence of Functionals on Density Funcational Theory Calculations of the Properties of Reducible Transitions Metal Oxide Catalysts. *J. Phys. Chem. C* **2013**, *117*, 25562-25578.

[39] Perdew, J.P.; Burke, K.; Ernzerhof, M. Generalized Gradient Approximation Made Simple. *Phys. Rev. Lett.* **1996**, *77* (18), 3865-3868.

[40] Zhao, Y.; Truhlar, D.G. A New Local Density Functional for Main-Group Thermochemistry, Transition Metal Bonding, Thermochemical Kinetics, and Noncovalent Interactions. *J. Chem. Phys.* **2006**, *125*, 194101.

[41] Kresse, G.; Furthmüller, J. Efficient Iterative Schemes for Ab Initio Total-Energy Calculations Using a Plane-Wave Basis Set. *Phys. Rev. B* **1996**, *54*, 11169.

[42] Blochl, P.E. Projector-Augmented Wave Method. *Phys. Rev. B* **1994**, *50*, 17953.

[43] L. Kihlborg, Arkiv. Kemi 21 (1963) 357.

[44] Tyuterev, V.G.; Vast, N. Murnaghan's Equation of State for the Electronic Ground State Energy. *Comput. Mater. Sci.* **2006**, *38*, 350-353.

[45] Zeng, H.C.; Lim, L.C. Secondary Ionic Forces in Lead Molybdate Melt Solidification. *J. Mater. Res.* **1998**, *13* (6), 1426-1429.

[46] Wheeler, S.E.; Houk, K.N. Integration Grid Errors for Meta-GGA-Predicted Reaction Energies. *J. Chem. Theory Comput.* **2010**, *6*, 395-404.

[47] Sleight, A.W.; Aykan, K.; Rogers, D.B. New Nonstoichiometric Molybdate, Tungstate, and Vanadate Catalysts with the Scheelite-Type Structure. *J. Solid State Chem.* **1975**, *13*, 231-236.

[48] Shao, Y; Gan, Z.; Epifanovsky, E.; Gilbert, A.T.B.; Wormit, M.; Kussmann, J.; Lange, A.W.; Behn, A.; Deng, J.; Feng, X.; et al. Advances in Molecular Quantum Chemistry Contained in the Q-Chem 4 Program Package. *Mol. Phys.* **2015**, *113*, 184-215.

[49] Andrae, D.; Häußermann, U.; Dolg, M.; Stoll, H.; Preuss, H.; Energy-Adjusted Ab Initio Pseudopotentials for the Second and Third Row Transition Elements. *Theor. Chim. Acta.* **1990**, *77*, 123-141.
[50] Schuchardt, K.L.; Didier, B.T.; Elsethagen, T.; Sun, L.; Gurumoorthi, V.; Chase, J.; Li, J.; Windus, T.L. Basis Set Exchange: A Community Database for Computational Sciences. *J. Chem. Inf. Model.* **2007**, *47*, 1045-1052.
[51] Chai, J.-D.; Head-Gordon, M. Systematic Optimization of Long-Range Corrected Hybrid Density Functionals. *J. Chem. Phys.* **2010**, *128*, 084106.
[52] Schaftenaar, G.; Noordik, J.H. Molden: a Pre- and Post-Processing Program for Molecular and Electronic Structures. *J. Comput.-Aided Mol. Design*, **2000**, *14*, 123-134.
[53] Momma, K.; Izumi, F. VESTA 3 for Three-Dimensional Visualization of Crystal, Volumetric and Morphology Data. *J. Appl. Crystallogr.* **2011**, *44* (6), 1272-1276.
[54] Kwapien, K.; Sierka, M.; Dobler, J.; Sauer, J. Reactions of H_2, CH_4, C_2H_6, and C_3H_8 with $[(MgO)_n]^+$ Clusters Studied by Density Functional Theory. *Chem. Cat. Chem.* **2010**, *2* (7), 819-826.
[55] Sinev, M.Y.; Fattakhova, Z.T.; Lomonosov, V.I.; Gordienko, Y.A. Kinetics of Oxidative Coupling of Methane: Bridging the Gap Between Comprehension and Description. *J. Nat. Gas Chem.* **2009**, *18*, 273-287.
[56] J. Yu, Y. Xu, V. Guliants, Propane Ammoxidation over Mo-V-TeNb-O M1 phase: Density Functional Theory Study of Propane Oxidative Dehydrodgenation Steps. *Catal. Today* **2014**, *238*, 28-34.
[57] R.A. Wheeler, P.N.V. Pavan Kumar, Stereochemically Active or Inactive Lone Pair Electrons in some Six-Coordinate, Group 15 Halides. *J. Am. Chem. Soc.* **1992**, *114*, 4776-4784.
[58] Walsh, A.; Watson, W.G.; Payne, D.G.; Egdell, R.G.; Guo, J.; Glans, P.-A.; Learmonth, T.; Smith, K.E. *Phys. Rev. B* **2006**, *73* (23), 235104.
[59] Volta, J.-C.; Forissier, M.; Theobald, F.; Pham, T.P. Dependence of Selectivity on Surface Structure of MoO_3 Catalysts. *Royal Soc. Chem.* **1981**, 225-233.

TOC Graphic

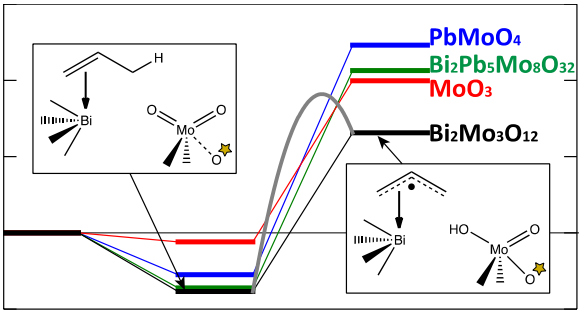
PbMoO4
Bi2Pb5Mo8O32
MoO3
Bi2Mo3O12
H
Bi
O
Mo
O
O
HO
Bi
Mo
O
O